Design, Synthesis, and Mechanistic Investigations of Bile Acid–Tamoxifen Conjugates for Breast Cancer Therapy

ARTICLE *in* BIOCONJUGATE CHEMISTRY · AUGUST 2013

Impact Factor: 4.51 · DOI: 10.1021/bc300664k · Source: PubMed

9 AUTHORS, INCLUDING:

Sreekanth Vedagopuram
Regional Centre for Biotechnology
10 PUBLICATIONS **47** CITATIONS
SEE PROFILE

Sandhya Bansal
University of Illinois, Urbana-Champaign
13 PUBLICATIONS **100** CITATIONS
SEE PROFILE

Rajender K Motiani
Institute of Genomics and Integrative Biology
29 PUBLICATIONS **906** CITATIONS
SEE PROFILE

Panjamurthy Kuppusamy
NIDDK Project, MD
23 PUBLICATIONS **381** CITATIONS
SEE PROFILE

Bioconjugate Chemistry

Article

pubs.acs.org/bc

Design, Synthesis, and Mechanistic Investigations of Bile Acid–Tamoxifen Conjugates for Breast Cancer Therapy

Vedagopuram Sreekanth,[†,§] Sandhya Bansal,[†,§] Rajender K. Motiani,[†] Somanath Kundu,[†] Sravan Kumar Muppu,[†] Tapodhara Datta Majumdar,[†] Kuppusamy Panjamurthy,[†] Sagar Sengupta,[‡] and Avinash Bajaj*[,†]

[†]The Laboratory of Nanotechnology and Chemical Biology, Regional Centre for Biotechnology, 180 Udyog Vihar, Phase 1, Gurgaon-122016, Haryana, India

[‡]National Institute of Immunology, Aruna Asaf Ali Marg, New Delhi 110067, India

Supporting Information

ABSTRACT: We have synthesized two series of bile acid tamoxifen conjugates using three bile acids lithocholic acid (**LCA**), deoxycholic acid (**DCA**), and cholic acid (**CA**). These bile acid–tamoxifen conjugates possess 1, 2, and 3 tamoxifen molecules attached to hydroxyl groups of bile acids having free acid and amine functionalities at the tail region of bile acids. The *in vitro* anticancer activities of these bile acid–tamoxifen conjugates show that the free amine headgroup based cholic acid–tamoxifen conjugate (**CA-Tam$_3$-Am**) is the most potent anticancer conjugate as compared to the parent drug tamoxifen and other acid and amine headgroup based bile acid–tamoxifen conjugates. The cholic acid–tamoxifen conjugate (**CA-Tam$_3$-Am**) bearing three tamoxifen molecules shows enhanced anticancer activities in both estrogen receptor +ve and estrogen receptor −ve breast cancer cell lines. The enhanced anticancer activity of **CA-Tam$_3$-Am** is due to more favorable irreversible electrostatic interactions followed by intercalation of these conjugates in hydrophobic core of membrane lipids causing increase in membrane fluidity. Annexin-FITC based FACS analysis showed that cells undergo apoptosis, and cell cycle analysis showed the arrest of cells in sub G_0 phase. ROS assays showed a high amount of generation of ROS independent of ER status of the cell line indicating changes in mitochondrial membrane fluidity upon the uptake of the conjugate that further leads to the release of cytochrome *c*, a direct and indirect regulator of ROS. The mechanistic studies for apoptosis using PCR and western analysis showed apoptotsis by intrinsic and extrinsic pathways in ER +ve MCF-7 cells and by only an intrinsic pathway in ER −ve cells. *In vivo* studies in the 4T1 tumor model showed that **CA-Tam$_3$-Am** is more potent than tamoxifen. These studies showed that bile acids provide a new scaffold for high drug loading and that their anticancer activities strongly depend on charge and hydrophobicity of lipid–drug conjugates.

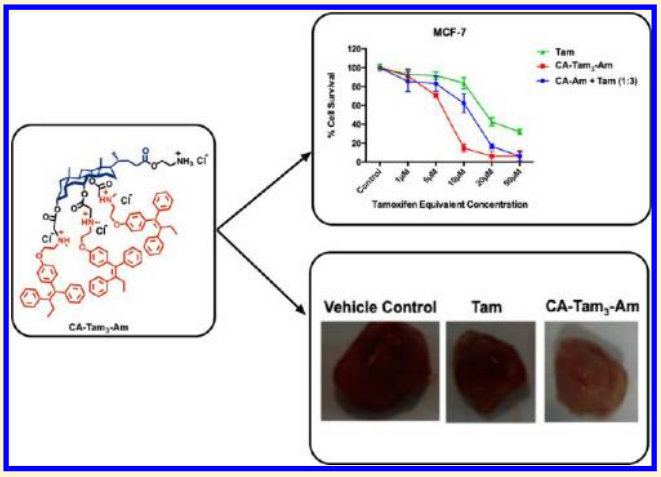

INTRODUCTION

Cancer chemotherapy aims for the specific delivery of chemotherapeutic drugs to target cancer cells leading to the destruction of primary tumors in the body.[1] Chemotherapy for cancer is associated with challenges and complications like the (1) inability of drug molecules to cross the biological barriers; (2) poor specificity leading to the advent of several side effects; (3) low accumulation of drugs inside cancer cells; and (4) rapid development of resistance of cancer cell to chemotherapeutic drugs.[2] To overcome these challenges, drug delivery systems like liposomes, polymers, dendrimers, and nanoparticles have been developed for the effective delivery of chemotherapeutic drugs.[3] Clinically, low outputs of existing drug delivery systems stress upon the development of better drug delivery vehicles and understanding the mechanisms of these delivery vehicles.

Breast cancer is the second leading cause of cancer deaths today after lung cancer and is the most common cancer among women.[4] Tamoxifen belongs to a class of nonsteroidal triphenylethylene derivatives and is the first selective estrogen receptor modulator (SERM). Tamoxifen shows its potential effects in patients who possess estrogen receptor (ER) positive (+ve) cancer cells by competing with estrogen for estrogen receptors. Regardless of estrogen receptor status, tamoxifen has also been useful for the treatment of women with early stage breast cancers as it shows cytotoxic effects toward ER +ve and ER negative (−ve) tumor cells.[5] The major challenge of

Received: December 13, 2012
Revised: July 9, 2013
Published: August 5, 2013

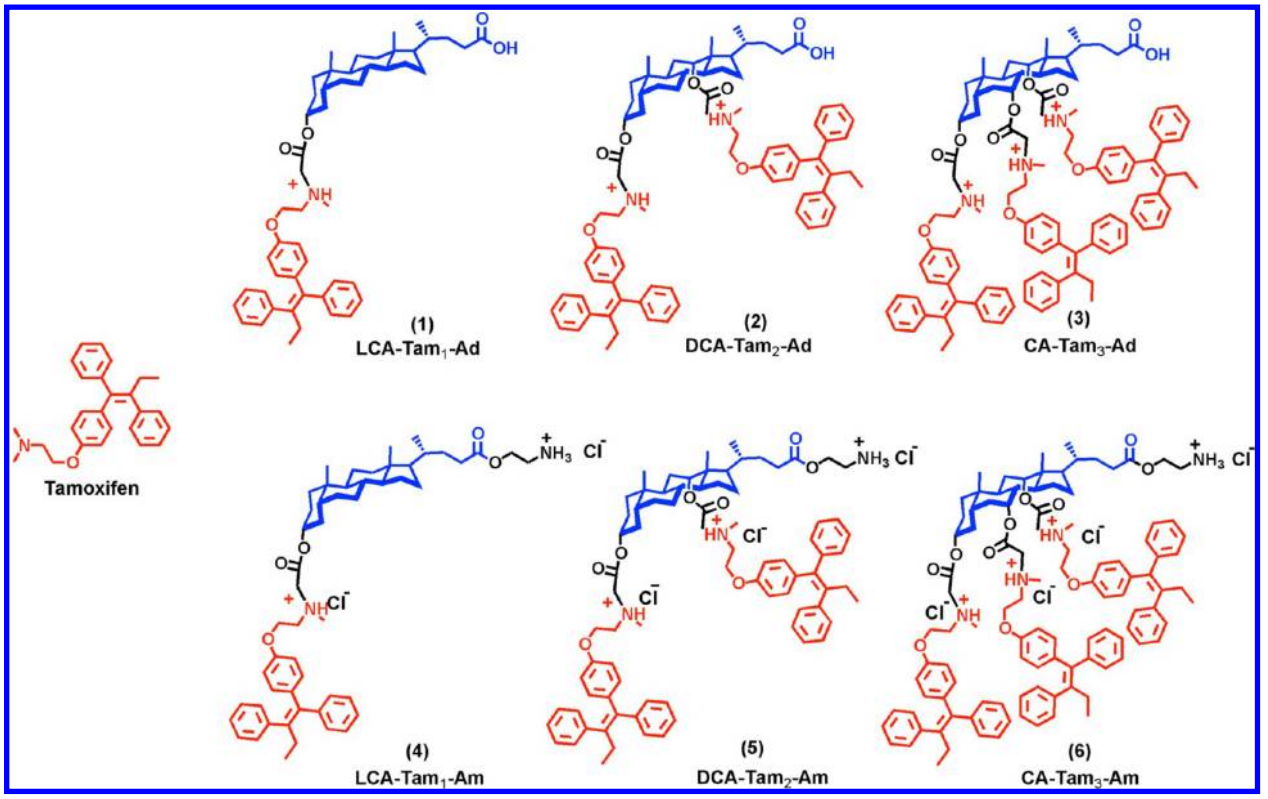

Figure 1. Molecular structures of **Tam**, **LCA-Tam$_1$-Ad**, **DCA-Tam$_2$-Ad**, **CA-Tam$_3$-Ad**, **LCA-Tam$_1$-Am**, **DCA-Tam$_2$-Am**, and **CA-Tam$_3$-Am** used in this study.

commercialized tamoxifen citrate is its poor oral bioavailability, high hepatic and intestinal first pass metabolism, hepatotoxicities, and a high risk of endometrial cancer.[6]

Lipid−drug conjugates can provide alternative drug delivery vehicles to overcome the challenges and complications of existing anticancer drugs. Covalent conjugation of drugs to lipid molecules with labile linkages would help in controlled drug release from lipid−drug conjugates and would increase the efficacy of drug loading capacity. Lipid−drug conjugates provide better cellular penetration, controlled drug release, better pharmacokinetics, improved tumor accumulation, and better cellular penetration leading to enhanced therapeutic activity and lower toxicity. Sengupta et al. have recently reported the conjugation of cisplatin to cholesterol and its liposomal formulation for anticancer activities.[7] The efficiency of lipid-anticancer drugs depends on lipid's carbon chain length, configuration of double bonds, location, and the nature of covalent linkage with the drug. Chikkara and co-workers have synthesized a library of lipid drug conjugates and explored for anticancer[8] and anti-HIV activities.[9] Banerjee et al. studied cationic lipid-haloperidol conjugates[10] and lipid-modified estrogen derivatives for treatment of breast cancer.[11]

The amount of drug loading in a carrier and its surface characteristics are very important parameters in cancer chemotherapy. The rigid steroidal backbone, facial amphiphilic character, chemically different hydroxyl groups, enantiomeric purity, low costs, and availability make bile acids ideal building blocks for drug delivery applications.[12] Bile acids offer structural advantages for the conjugation of drugs using their −OH and −COOH functional groups. Polli et al. have shown the increased oral bioavailability of acyclovir on conjugation with bile acid.[13] Similarly, cholic acid−cisplatin conjugates were tested for their anticancer activities in human cancer cell lines.[14] Facial amphiphilic character of bile acids including the hydrophobic backbone can be used to explore the micelle-based nanoparticles for drug encapsulation and anticancer therapy. Wang and co-workers have synthesized a biocompatible amphiphilic telodendrimer system based on cholic acid and explored its self-assemblies for efficient delivery of paclitaxel in different tumor models.[15]

The major challenge in cancer drug delivery is the decreased amount of drug uptake and accumulation in cancer cells. One of the ways to tackle the drug accumulation problem is to use a suitable carrier that has maximum drug loading capacity. The chemistry and biology of a drug carrier play a key role in selective delivery and intratumoral accumulation of the drug. Covalent linkage of drugs to the carrier will add advantages to its delivery. Endogenous bile acids offer such advantages with good drug conjugating capacity, and it can be modified with different head groups that would help in effective interactions with cells to improve intracellular accumulation of drugs. In this article, we present the conjugation strategies for the synthesis of bile acid−tamoxifen conjugates possessing acid and amine head groups with the anticipation that amine head groups will interact better than acid head groups that would further help in the intracellular accumulation of these conjugates. These conjugates were then explored for anticancer activities in three estrogen +ve 4T1, MCF-7, and T47D, and one estrogen −ve MDA-MB-231 cell line. The interactions of bile acid−tamoxifen conjugates with model membranes were studied using surface plasmon resonance (SPR) and DPH based fluorescence anisotropic studies to explore the differential activities of bile acid−tamoxifen conjugates. Then, we explored the mechanism of anticancer activities using Annexin-FITC, cell cycle assay, ROS generation assay, PCR, and Western blotting

dx.doi.org/10.1021/bc300664k | *Bioconjugate Chem.* 2013, 24, 1468−1484

Scheme 1. Synthesis of Bile Acid−Tamoxifen Conjugates Bearing Acid Head Groups[a]

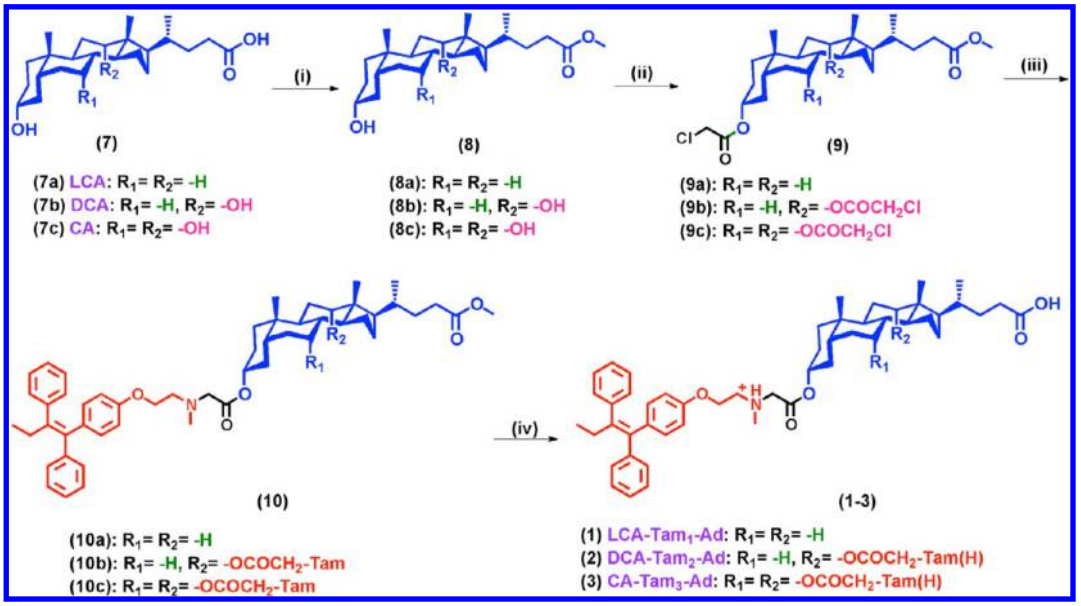

[a]Reagents, reaction conditions, and yields: (i) MeOH, conc. HCl, RT, 12 h, 98%; (ii) chloroacetic anhydride, pyridine, DMAP, toluene, 90 °C, 12 h, 80−88%; (iii) *N*-desmethyl tamoxifen, TEA, acetonitrile, reflux, 16 h, 65−70%; (iv) 2 M NaOH, 1:1 THF-acetonitrile, 0 °C to RT, 6 h, 40−48%.

studies. The *in vivo* potential of bile acid−tamoxifen conjugate was then explored in 4T1 tumor models.

EXPERIMENTAL SECTION

Materials and Methods. All of the solvents and chemicals used are of ACS grade. Lithocholic acid (LCA), deoxycholic acid (DCA), cholic acid (CA), tamoxifen, chloroacetic anhydride, diphenylhexatriene (DPH), and octyl glucoside were purchased from Sigma-Aldrich. The HPA chip was obtained from GE Healthcare, USA. DPPC was purchased from Avanti Polar Lipids, USA. Unless mentioned, all of the compounds were purified using Combi-flash chromatography using silica gel redi-sep columns. All of the ^{1}H NMR spectra were recorded on a Bruker-Avance-500 MHz FT-NMR spectrometer. Chemical shifts are reported in δ ppm reference to $CDCl_3$ for ^{1}H NMR. All of the mass spectra were recorded with an AB SCIEX Triple TOF 5600 system.

Synthesis of *N*-Desmethyltamoxifen. Tamoxifen (0.53 g, 1.43 mmol) was dissolved in anhydrous dichloroethane (15 mL) at 0 °C followed by the addition of 2-chloroethyl chloroformate (0.17 mL, 1.49 mmol) and allowed to stir for 15 min. The reaction mixture was refluxed for 24 h, and the solvent was evaporated to obtain yellowish oil. This yellowish oil was dissolved in methanol (10 mL), and the reaction mixture was refluxed for ∼3 h. The solvent was evaporated, and the reaction mixture was purified by column chromatography using 230−400 mesh silica gel, with solvent system 10:1 CH_2Cl_2/CH_3OH to obtain 0.52 g (91%) of *N*-desmethyl tamoxifen. ^{1}H NMR (DMSO-d_6, 500 MHz) δ 0.84 (3H, t, J = 7.2 Hz), 2.37 (2H, q, J = 14.8, 7.6 Hz), 2.56 (3H, s), 3.12 (2H, t, J = 4.8 Hz), 4.08 (2H, t, J = 4.8 Hz), 6.65 (2H, d, J = 8.8 Hz), 6.77 (2H, d, J = 8.8 Hz), 7.14−7.38 (10H, m), 8.8 (1H, br); HRMS (ESI) $(C_{25}H_{27}NO)^+$ calcd, 358.2171; found, 358.21.

Synthesis of Bile Acid−Tamoxifen Conjugates Bearing Acid Groups (1−3) (Scheme 1). *General Procedure for the Synthesis of Bile Acid Methyl Esters (**8a/8b/8c**).* Bile acid (**7a**/**7b**/**7c**) (10 mmol) was dissolved in anhydrous methanol (50 mL); conc. HCl (5 mL) was added to it, and the reaction mixture was stirred for 12 h at room temperature. After 12 h, the solvent was evaporated; the mixture was diluted with dichloromethane (150 mL) and washed with $NaHCO_3$ solution (2 × 20 mL) and brine (2 × 10 mL). The organic phase was dried over anhydrous Na_2SO_4, and the solvent was evaporated in vacuum. The colorless crystalline solid obtained was taken for further reaction without any purification.

*Methyl 3α-Hydroxy-5β-lithocholan-24-oate (**8a**).* Yield 98%. ^{1}H NMR (500 MHz, $CDCl_3$): δ 0.67 (3 H, s, C_{18}-CH_3), 0.97−1.96 (m), 2.18−2.28 (1 H, m), 2.32−2.40 (1 H, m), 3.40−3.44 (1 H, m, C_3-CH), 3.66 (3 H, s, −CO-OCH_3). HRMS (ESI): m/z $(C_{25}H_{42}O_3)^+$ calcd, 390.3134; found, 390.3284 (M^+), 413.2949 $(M + Na)^+$.

*Methyl 3α,12α-Dihydroxy-5β-deoxycholan-24-oate (**8b**).* Yield 98%. ^{1}H NMR (500 MHz, $CDCl_3$): δ 0.67 (3 H, s, C_{18}-CH_3), 0.91 (3 H, s, C_{19}-CH_3), 0.97 (3 H, d, J = 4.5 Hz, C_{21}-CH_3), 1.07−1.83 (m), 2.21−2.28 (1 H, m), 2.35−2.41 (1H, m, C_3-CH), 3.66 (3 H, s, −CO-OCH_3), 3.98 (1H, s, C_{12}-CH). HRMS (ESI): m/z $(C_{25}H_{42}O_4)^+$ calcd, 406.3083; found, 407.3088 $(M + H)^+$, 429.2903 $(M + Na)^+$.

*Methyl 3α,7α,12α-Trihydroxy-5β-cholan-24-oate (**8c**).* Yield 98%. ^{1}H NMR (500 MHz, $CDCl_3$): δ 0.67 (3 H, s, C_{18}-CH_3), 0.88 (3 H, s, C_{19}-CH_3), 0.97 (3 H, d, J = 6.1 Hz, C_{21}-CH_3), 1.24−2.36 (m), 3.40−3.44 (1 H, m, C_3-CH), 3.66 (3 H, s, −CO-OCH_3), 3.84 (1 H, s, C_{12}-CH), 3.96 (1 H, s, C_7-CH). HRMS (ESI): m/z $(C_{25}H_{42}O_5)^+$ calcd, 422.3032; found, 423.3038 $(M + H)^+$.

*General Procedure for the Synthesis of (2′-Chloro)acetoxy Derivatives of Bile Acid Methyl Esters (**9a/9b/9c**).* To a solution of compound (**8a**/**8b**/**8c**) (5 mmol) in toluene (25 mL), pyridine (2 mL) and DMAP (0.25 mmol) were added and stirred at room temperature for 30 min. To this reaction mixture, a solution of chloroacetic anhydride (1.2 equiv for **8a**; 2.4 equiv for **8b**; and 3.6 equiv for **8c**) in toluene (5 mL) was added, then the reaction mixture was heated to 90 °C for 12 h. The solvent was evaporated in vacuum, diluted with dichloromethane (50 mL), and washed with brine solution (2 × 20 mL). The organic phase was dried over anhydrous Na_2SO_4 and

dx.doi.org/10.1021/bc300664k | *Bioconjugate Chem.* 2013, 24, 1468−1484

Scheme 2. Synthesis of Bile Acid−Tamoxifen Conjugates Bearing Amine Head Groups[a]

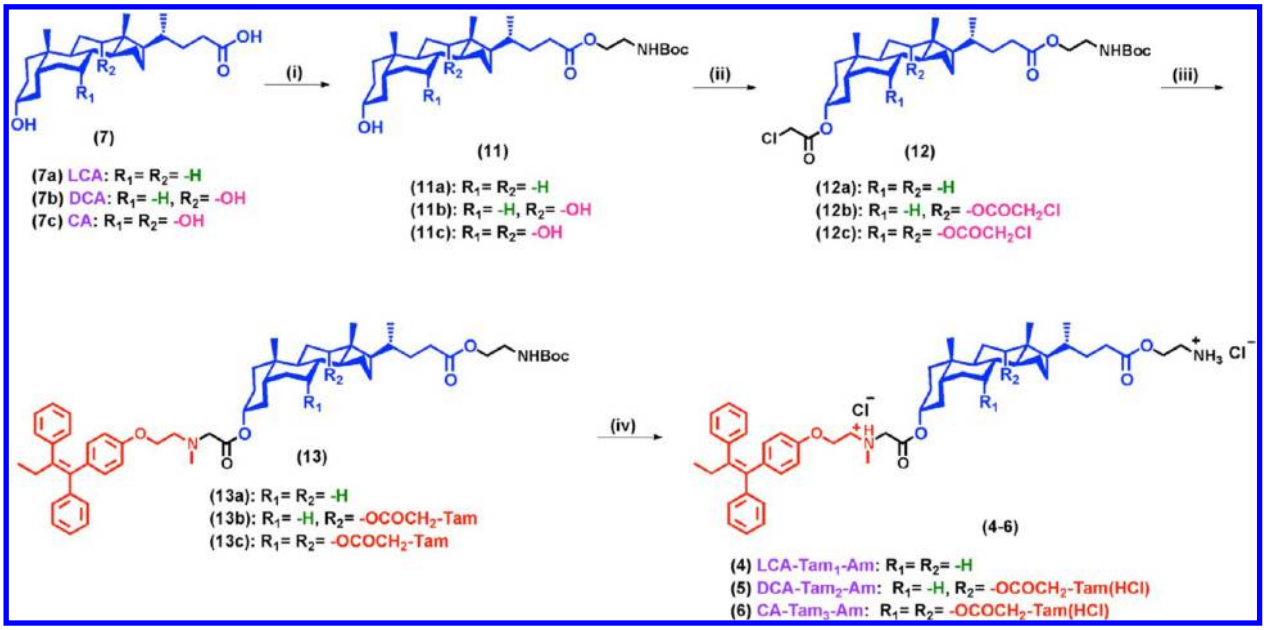

[a]Reagents, reaction conditions, and yields: (i) NHS, EDC·HCl, DMF, RT, 8 h, *N*-bocethanolamine, RT, 12 h, 78−85%; (ii) chloroacetic anhydride, pyridine, DMAP, toluene, 90 °C, 12 h, 76−90%; (iii) *N*-desmethyl tamoxifen, TEA, acetonitrile, reflux, 16 h, 68−80%; (iv) TFA, CH_2Cl_2, 0 °C to RT, 6 h, 96−98%, amberlyte IRA-900, MeOH, RT, 8 h.

evaporated in vacuum. The crude product was purified by silica gel (230−400 mesh) combi-flash column chromatography using ethyl acetate-pet ether as eluent to obtain a colorless solid.

*Methyl 3α-(2′-Chloro)acetoxy-5β-lithocholan-24-oate (**9a**).* Yield 88%. ^{1}H NMR (500 MHz, $CDCl_3$): δ 0.64 (3 H, s, C_{18}-CH_3), 0.90−1.97 (m), 2.17−2.21 (6 H, m), 2.35−2.40 (1 H, m), 3.66 (3 H, s, −CO-O-CH_3), 4.03 (2 H, s, −CO-CH_2-Cl), 4.76−4.85 (1 H, m, C_3-CH). HRMS (ESI): *m/z* $(C_{27}H_{43}O_4Cl)^+$ calcd, 466.2850; found, 466.3469 (M^+), 489.2664 $(M + Na)^+$.

*Methyl 3α,12α-di(2′-Chloro)acetoxy-5β-deoxycholan-24-oate (**9b**).* Yield 85%. ^{1}H NMR (500 MHz, $CDCl_3$): δ 0.74 (3 H, s, C_{18}-CH_3), 0.78 (3 H, d, *J* = 6.5 Hz, C_{21}-CH_3), 0.923 (3 H, s, C_{19}-CH_3), 1.03−1.89 (m), 2.30−2.39 (1 H, m), 2.17−2.25 (1 H, m), 3.66 (3 H, s, −CO-OCH_3), 4.03 (2 H, s, −CO-CH_2-Cl), 4.07 (2 H, s, −CO-CH_2-Cl), 4.13 (2 H, s), 4.75−4.83 (1 H, m, C_3-CH), 5.19 (1 H, s, C_{12}-CH). HRMS (ESI): *m/z* $(C_{29}H_{44}O_6Cl_2)^+$ calcd, 558.2515; found, 581.2356 $(M + Na)^+$.

*Methyl 3α,7α,12α-tri(2′-Chloro)acetoxy-5β-cholan-24-oate (**9c**).* Yield 80%. ^{1}H NMR (500 MHz, $CDCl_3$): δ 0.75 (3 H, s, C_{18}-CH_3), 0.83 (3 H, d, *J* = 6.0 Hz, C_{21}-CH_3), 0.94 (3 H, s, C_{19}-CH_3), 1.09−2.20 (m), 2.30−2.40 (1 H, m), 3.65 (3 H, s, −CO-OCH_3), 4.02−4.12 (6 H, m, 3 × −CO-CH_2-Cl), 4.64−4.74 (1 H, m, C_3-CH), 5.04 (1 H, s, C_7-CH), 5.20 (1 H, s, C_{12}-CH). HRMS (ESI): *m/z* $(C_{31}H_{45}O_8Cl_3)^+$ calcd, 650.2184; found, 672.2405 $(M + Na)^+$.

*General Procedure for the Conjugation of Tamoxifen to Bile Acid Methyl Esters (**10a/10b/10c**).* To a solution of compound (**9a**/**9b**/**9c**) (3 mmol) in acetonitrile (15 mL), triethylamine (2 mL) and desmethylated tamoxifen (1.1 equiv for **9a**; 2.2 equiv for **9b**; and 3.3 equiv for **9c**) was added, and the reaction mixture was refluxed for 16 h. The solvent was evaporated in vacuum, diluted with DCM (50 mL), and washed with brine solution (2 × 10 mL). The organic phase was dried over anhydrous Na_2SO_4 and evaporated in vacuum. The crude product was purified by silica gel (230−400 mesh) combi-flash column chromatography using ethyl acetate-pet ether as eluent to obtain a colorless solid.

*Compound (**10a**).* Yield 70%. ^{1}H NMR (500 MHz, $CDCl_3$): δ 0.63 (3 H, s, C_{18}-CH_3), 0.86−1.98 (m), 2.17−2.25 (9H, m), 2.31−2.39 (1 H, m), 2.45 (5 H, s), 2.91 (2 H, t, *J* = 5.0 Hz, -N-CH_2), 3.33 (2 H, s, −CO-CH_2-N), 3.66 (3 H, s, −CO-OCH_3), 3.95 (2 H, t, *J* = 5.5 Hz, 2 × -O-CH_2-), 4.73−4.81 (1 H, m, C_3-CH), 6.54 (2 H, d, *J* = 8.5 Hz, 2 × Ar-CH), 6.75 (2 H, d, *J* = 8.5 Hz, 2 × −O-Ar-CH), 7.11−7.34 (10 H, m, 2 × C_6H_5). HRMS (ESI): *m/z* $(C_{52}H_{69}O_5N)^+$ calcd, 787.5176; found 788.5660 $(M + H)^+$.

*Compound (**10b**).* Yield 65%. ^{1}H NMR (500 MHz, $CDCl_3$): δ 0.718−1.91 (m), 2.04 (2 H, s), 2.17 (3 H, m), 2.27−2.32 (1 H, m), 2.37 (3 H, s), 2.45 (6 H, s), 2.81−2.97 (4 H, m), 3.25 (2 H, s), 3.39 (2 H, s), 3.63 (3 H, s), 3.89 (2 H, t, *J* = 5.5 Hz), 3.93 (2 H, t, *J* = 6 Hz), 4.10−4.14 (1 H, m), 4.69−4.74 (1 H, m, C_3-CH), 5.14 (1 H, s, C_{12}-CH), 6.51 (4 H, d, *J* = 8.5 Hz, 4 × Ar-CH), 6.74 (4 H, d, *J* = 8.5 Hz, 4 × −O-Ar-CH), 7.10−7.33 (20 H, m, 4 × C_6H_5). HRMS (ESI): *m/z* $(C_{79}H_{96}O_8N_2)^+$ calcd, 1200.7167; found, 1201.7870 $(M + H)^+$.

*Compound (**10c**).* Yield 70%. ^{1}H NMR (500 MHz, $CDCl_3$): δ 0.71 (3 H, s, C_{18}-CH_3), 0.77−2.32 (m), 2.36 (3 H, s), 2.45 (9 H, s, 3 × -N-CH_3), 2.79−2.91 (6 H, m, 3 × -N-CH_2), 3.20−3.45 (6 H, m, 3 × −CO-CH_2-N-), 3.61 (3 H, s, −CO-OCH_3), 3.84−3.90 (6 H, m, 3 × -O-CH_2-), 4.54−4.63 (1 H, m, C_3-CH), 4.95 (1 H, s, C_7-CH), 5.17 (1 H, s, C_{12}-CH), 6.49 (6 H, d, *J* = 8.0 Hz, 3 × Ar-CH), 6.73 (6 H, d, *J* = 8.0 Hz, 6 × −O-Ar-CH), 6.74−7.32 (30 H, m, 6 × C_6H_5). HRMS (ESI): *m/z* $(C_{106}H_{123}O_{11}N_3)^+$ calcd, 1613.9158; found, 1615.0201 $(M + H)^+$.

*General Procedure for Ester Hydrolysis (**1/2/3**).* To a solution of compound (**10a**/**10b**/**10c**) (1.5 mmol) in 1:1 acetonitrile−THF (10 mL), 2 M NaOH (2 mL) was added dropwise at 0 °C, and the reaction was continued at room temperature for about 6 h. The solvent was evaporated in

dx.doi.org/10.1021/bc300664k | *Bioconjugate Chem.* 2013, 24, 1468−1484

vacuum, and the residue was diluted with DCM (25 mL) and washed with 2 N HCl solution (2 × 3 mL) and brine solution (2 × 5 mL). The organic phase was dried over anhydrous Na_2SO_4 and evaporated *in vacuo*. The crude product was purified by silica gel (230−400 mesh) combi-flash column chromatography using ethyl acetate-pet ether as eluent to obtain a colorless solid.

*Compound (**1**).* Yield 45%. ^{1}H NMR ($CDCl_3$, 500 MHz) δ 0.64 (3 H, s, C_{18}-CH_3), 0.86−1.89 (m), 2.17−2.25 (9 H, m), 2.31−2.39 (1 H, m), 2.45 (5 H, s), 2.91 (2 H, t, J = 5.0 Hz, -N-CH_2), 3.33 (2 H, s, −CO-CH_2-N), 3.95 (2 H, t, J = 5.5 Hz, 2 × -O-CH_2-), 4.73- 4.81 (1 H, m, C_3-CH), 6.54 (2 H, d, J = 8.5 Hz, 2 × Ar-CH), 6.75 (2 H, d, J = 8.5 Hz, 2 × −O-Ar-CH), 7.11−7.34 (10 H, m, 2 × C_6H_5). MS (ESI): m/z $(C_{51}H_{67}O_5N)^+$ calcd, 773.5; found, 773.4 (M^+).

*Compound (**2**).* Yield 40%. ^{1}H NMR (500 MHz, $CDCl_3$): δ 0.718−1.91 (m), 2.04 (2 H, s), 2.17 (3 H, m), 2.27−2.32 (1 H, m), 2.37 (3 H, s), 2.45 (6 H, s), 2.81−2.97 (4 H, m), 3.25 (2 H, s), 3.39 (2 H, s), 3.89 (2 H, t, J = 5.5 Hz), 3.93 (2 H, t, J = 6 Hz), 4.10−4.14 (1 H, m), 4.69−4.74 (1 H, m), 5.14 (1 H, s), 6.51 (4 H, d, J = 8.5 Hz, 4 × Ar-CH), 6.74 (4 H, d, J = 8.5 Hz, 4 × −O-Ar-CH), 7.10−7.33 (20 H, m, 4 × C_6H_5). HRMS (ESI): m/z $(C_{78}H_{94}O_8N_2)^+$ calcd, 1186.701; found, 1187.5 (M + H)$^+$.

*Compound (**3**).* Yield 48%. ^{1}H NMR ($CDCl_3$, 500 MHz) δ 0.71 (3 H, s, C_{18}-CH_3), 0.77−2.32 (m), 2.36 (3 H, s), 2.45 (9 H, s, 3 × -N-CH_3), 2.79−2.91 (6 H, m, 3 × -N-CH_2), 3.20−3.45 (6 H, m, 3 × −CO-CH_2-N-), 3.84- 3.90 (6 H, m, 3 × -O-CH_2-), 4.54−4.63 (1 H, m, C_3-CH), 4.95 (1 H, s, C_7-CH), 5.17 (1 H, s, C_{12}-CH), 6.49 (6 H, d, J = 8.0 Hz, 3 × Ar-CH), 6.73 (6 H, d, J = 8.0 Hz, 6 × −O-Ar-CH), 6.74−7.32 (30 H, m, 6 × C_6H_5). MS (ESI): m/z $(C_{105}H_{121}O_{11}N_3)^+$ calcd, 1599.9; found, 1600.9 (M + H)$^+$.

Synthesis of Bile Acid−Tamoxifen Conjugates with Amine Head Groups (4−6) (Scheme 2). *General Procedure for the Synthesis of Bile Acid Boc-ethanolamine Esters (**11a/11b/11c**).* Bile acid (**7a**/**7b**/**7c**) (3 mmol) was dissolved in anhydrous DMF (20 mL); *N*-hydroxysuccinamide (3.3 mmol, 1.1 equiv.) and EDC·HCl (3.3 mmol, 1.1 equiv.) were added to it; and the reaction mixture was stirred at room temperature for 8 h. A solution of *N*-Boc-ethanolamine (3.3 mmol) in anhydrous DMF (5 mL) was added, and the mixture was stirred for 12 h at room temperature. The solvent was evaporated, and the mixture was diluted with dichloromethane and washed with saturated $NaHCO_3$ solution (2 × 10 mL) and brine (2 × 10 mL). The organic phase was dried over anhydrous Na_2SO_4, and the solvent was evaporated under vacuum. The residue was purified by column chromatography on silica (230−400 mesh), using CH_2Cl_2/MeOH as eluent, to give a colorless solid.

*Lithocholic Acid Boc-ethanolamine Ester (**11a**).* Yield: 85%. ^{1}H NMR ($CDCl_3$, 500 MHz) δ 0.66 (3 H, s, C_{18}-CH_3), 0.91−2.0 (m), 2.49−2.75 (2 H, m), 2.81 (2 H, t, J = 4.5 Hz, -CH_2-NH-), 3.35 (2 H, t, J = 4.5 Hz, -O-CH_2-), 3.61−3.71 (1 H, m, C_3-CH). HRMS $(C_{31}H_{53}NO_5)^+$ calcd, 519.7562; found, 520.4 (M + H)$^+$.

*Deoxycholic Acid Boc-ethanolamine Ester (**11b**).* Yield: 78%. ^{1}H NMR ($CDCl_3$, 500 MHz) δ 0.66 (3 H, s, C_{18}-CH_3), 0.91−2.0 (m), 2.49−2.75 (2 H, m), 2.81 (2 H, t, J = 5.0 Hz, -CH_2-NH-), 3.35 (2 H, t, J = 5.0 Hz, -O-CH_2-), 3.61−3.71 (1 H, m, C_3-CH), 3.97 (1 H, s, C_{12}-CH). HRMS $(C_{31}H_{53}NO_6)^+$ calcd, 535.3873; found, 534.4 (M − H)$^+$.

*Cholic Acid Boc-ethanolamine Ester (**11c**).* Yield: 82%. ^{1}H NMR ($CDCl_3$, 500 MHz) δ 0.66 (3 H, s, C_{18}-CH_3), 0.91−2.0 (m), 2.49−2.75 (2 H, m), 2.81 (2 H, t, J = 5.0 Hz, -CH_2-NH-), 3.35 (2 H, t, J = 5.0 Hz, -O-CH_2-), 3.31−3.42 (1 H, m, C_3-CH), 3.78 (1 H, s, C_7-CH), 3.87 (1 H, s, C_{12}-CH). HRMS $(C_{31}H_{53}NO_7)^+$ calcd, 551.3822; found, 551.0 (M^+).

*Synthesis of Compounds (**12a/12b/12c**).* Compound (**11a**/**11b**/**11c**) (3 mmol) was dissolved in anhydrous toluene (10 mL) and anhydrous pyridine (2 mL). A catalytic amount of DMAP was added, and the mixture was stirred for 45 min at room temperature. A solution of chloroacetic anhydride (1.2 equiv for **11a**; 2.4 equiv for **11b**; and 3.6 equiv for **11c**) in anhydrous toluene (10 mL) was added, and the mixture was refluxed for 12 h at 90 °C. The reaction mixture was diluted with CH_2Cl_2 and washed with 1 M HCl solution (2 × 10 mL). The organic phase was dried over anhydrous Na_2SO_4, and the solvent was evaporated under vacuum. The residue was purified by column chromatography on silica (230−400 mesh) using petroleum ether/ethyl acetate as eluent, to give a colorless solid.

*Compound (**12a**).* Yield: 90%. ^{1}H NMR ($CDCl_3$, 500 MHz) δ 0.66 (3 H, s, C_{18}-CH_3), 0.91−2.0 (m), 2.49−2.75 (2 H, m), 2.81 (2 H, t, J = 4.5 Hz, -CH_2-NH-), 3.35 (2 H, t, J = 4.5 Hz, -O-CH_2-), 3.61−3.71 (1 H, m, C_3-CH), 4.03 (2 H, s, −CO-CH_2-Cl). HRMS $(C_{33}H_{54}NO_6Cl)^+$ calcd, 595.3640; found, 596.7 (M + H)$^+$.

*Compound (**12b**).* Yield: 82%. ^{1}H NMR ($CDCl_3$, 500 MHz) 0.66 (3 H, s, C_{18}-CH_3), 0.91−2.0 (m), 2.49−2.75 (2 H, m), 2.81 (2 H, t, J = 5.0 Hz, -CH_2-NH-), 3.35 (2 H, t, J = 5.0 Hz, -O-CH_2-), 3.61−3.71 (1 H, m, C_3-CH), 3.97 (1 H, s, C_{12}-CH), 4.03 (2 H, s, −CO-CH_2-Cl), 4.07 (2 H, s, −CO-CH_2-Cl). HRMS $(C_{35}H_{55}NO_8Cl_2)^+$ calcd, 687.3305; found, 686.0 (M − H)$^+$

*Compound (**12c**).* Yield: 76%. ^{1}H NMR ($CDCl_3$, 500 MHz) δ 0.66 (3 H, s, C_{18}-CH_3), 0.91−2.0 (m), 2.49−2.75 (2 H, m), 2.81 (2 H, t, J = 5.0 Hz, -CH_2-NH-), 3.35 (2 H, t, J = 5.0 Hz, -O-CH_2-), 3.31−3.42 (1 H, m, C_3-CH), 3.78 (1 H, s, C_7-CH), 3.87 (1 H, s, C_{12}-CH), 4.02−4.127 (6 H, m, 3 × −CO-CH_2-Cl). HRMS $(C_{37}H_{56}NO_{10}Cl_3)^+$ calcd, 779.2970; found, 782.0.

*Synthesis of Compounds (**13a/13b/13c**).* To solution of compound (**12a**/**12b**/**12c**) (3 mmol) in anhydrous acetonitrile (15 mL), 2 mL of triethylamine was added. A solution of *N*-desmethyl tamoxifen (1.1 equiv for **12a**; 2.2 equiv for **12b**; and 3.3 equiv for **12c**) in anhydrous acetonitrile (5 mL) was added to it, and the reaction mixture was refluxed for 16 h. The solvent was evaporated under vacuum, and the mixture was diluted with dichloromethane and washed with water (2 × 10 mL) and brine (2 × 10 mL). The organic phase was dried over anhydrous Na_2SO_4, and the solvent was evaporated under vacuum. The residue was purified by column chromatography on silica (230- 400 mesh), using petroleum ether/ethyl acetate as eluent, to give a colorless solid (**13a**/**13b**/**13c**).

*Compound (**13a**).* Yield: 80%. ^{1}H NMR ($CDCl_3$, 500 MHz) δ 0.71−1.91 (m), 2.04 (2 H, s), 2.17 (3 H, m), 2.27−2.32 (1 H, m), 2.37 (3 H, s), 2.45 (3 H, s, 1 × -N-CH_3), 2.81−2.97 (2 H, m, 1 × -N-CH_2), 3.25 (2 H, s, 1 × −CO-CH_2-N), 3.88−3.94 (2 H, m, 1 × -O-CH_2-), 4.69−4.74 (1 H, m, C_3-CH), 6.51 (2 H, d, J = 8.5 Hz, 2 × Ar-CH), 6.74 (2 H, d, J = 8.5 Hz, 2 × O−Ar-CH), 7.10−7.33 (10 H, m, 2 × C_6H_5). HRMS $(C_{31}H_{53}NO_5)^+$ calcd, 916.5966; found, 917.7 (M + H)$^+$.

*Compound (**13b**).* Yield: 76%. ^{1}H NMR ($CDCl_3$, 500 MHz) δ 0.65 (3H, s, C_{18}-CH_3), 0.93−2.55 (m), 2.54 (6 H, s, 2 × -N-CH_3), 2.81−2.94 (4 H, m, 2 × -N-CH_2), 3.2 (2 H, s, 1 × −CO-CH_2-N), 3.41 (2 H, s, 1 × −CO-CH_2-N), 3.61−3.69 (1 H, m, C_3-CH), 3.95 (2 H, t, J = 5.0 Hz, -O-CH_2), 4.08−4.16 (4 H, m,

dx.doi.org/10.1021/bc300664k | *Bioconjugate Chem.* 2013, 24, 1468−1484

2 × -O-CH_2-), 5.14 (1 H, s, C_{12}-CH), 6.49 (4 H, d, J = 8.5 Hz, 4 × Ar-CH), 6.72 (4 H, d, J = 8.5 Hz, 4 × O−Ar-CH), 7.12−7.4 (20 H, m, 4 × C_6H_5). HRMS $(C_{31}H_{53}NO_5)^+$ calcd, 1329.7956; found, 1330.9 $(M + H)^+$.

*Compound (**13c**).* Yield: 68%. ^{1}H NMR ($CDCl_3$, 500 MHz) δ 0.72 (3H, s, C_{18}-CH_3), 0.85−2.28 (m), 2.43 (9 H, s, 3 × -N-CH_3), 2.76−2.92 (6 H, m, 3 × -N-CH_2), 3.22 (2 H, s, 1 × −CO-CH_2-N), 3.34 (2 H, m, 1 × −CO-CH_2-N), 3.40 (2 H, s, 1 × −CO-CH_2-N), 3.85- 3.93 (6 H, m, 3 × -O-CH_2-), 4.5−4.61 (1 H, m, C_3-CH), 4.95 (1 H, s, C_7-CH), 5.17 (1 H, s, C_{12}-CH), 6.46 (6 H, d, J = 8.0 Hz, 3 × Ar-CH), 6.72 (6 H, d, J = 8.0 Hz, 6 × −O-Ar-CH), 6.78−7.36 (30 H, m, 6 × C_6H_5). HRMS $(C_{31}H_{53}NO_5)^+$ calcd, 1742.99; found, 1744.6 $(M + H)^+$.

*Synthesis of Compounds (**4/5/6**).* To a solution of compounds (**13a**/**13b**/**13c**) (2 mmol) in anhydrous DCM (10 mL), 4 mL of trifluoroacetic acid was added at 0 °C, and the reaction mixture was stirred at room temperature for 6 h. The solvent was evaporated under vacuum and precipitated out in hexane−ether mixture to give corresponding TFA salts as colorless solids. These TFA salts (0.25 mmol) were then dissolved in methanol (3 mL), Amberlite IRA-900 (1g) was added, and the mixture was stirred at room temperature for 8 h. The mixture was filtered, and the solid was washed with methanol (10 mL), the filtrate was evaporated to get the chloride exchanged colorless solid.

*Compound (**4**).* ^{1}H NMR ($CDCl_3$, 500 MHz) δ 0.71−1.91 (m), 2.04 (2 H, s), 2.17 (3 H, m), 2.27−2.32 (1 H, m), 2.37 (3 H, s), 2.45 (3 H, s, 1 × -N-CH_3), 2.81−2.97 (2 H, m, 1 × -N-CH_2), 3.25 (2 H, s, 1 × −CO-CH_2-N), 3.88−3.94 (2 H, m, 1 × -O-CH_2-), 4.69−4.74 (1 H, m, C_3-CH), 6.51 (2 H, d, J = 8.5 Hz, 2 × Ar-CH), 6.74 (2 H, d, J = 8.5 Hz, 2 × O−Ar-CH), 7.10−7.33 (10 H, m, 2 × C_6H_5). MS (ESI): m/z $(C_{78}H_{94}O_8N_2)^+$ calcd, 1186.7; found, 1187.5 $(M + H)^+$.

*Compound (**5**).* ^{1}H NMR ($CDCl_3$, 500 MHz) δ 0.65 (3H, s, C_{18}-CH_3), 0.93−2.55 (m), 2.54 (6 H, s, 2 × -N-CH_3), 2.81−2.94 (4 H, m, 2 × -N-CH_2), 3.2 (2 H, s, 1 × −CO-CH_2-N), 3.41 (2 H, s, 1 × −CO-CH_2-N), 3.61−3.69 (1 H, m, C_3-CH), 3.95 (2 H, t, J = 5.0 Hz, -O-CH_2), 4.08−4.16 (4 H, m, 2 × -O-CH_2-), 5.14 (1 H, s, C_{12}-CH), 6.49 (4 H, d, J = 8.5 Hz, 2 × Ar-CH), 6.72 (4 H, d, J = 8.5 Hz, 4 × O−Ar-CH), 7.12−7.4 (20 H, m, 4 × C_6H_5). MS (ESI): m/z $(C_{80}H_{99}N_3O_8)^+$ calcd, 1229.7; found, 1229.6 (M^+).

*Compound (**6**).* ^{1}H NMR ($CDCl_3$, 500 MHz) δ 0.72 (3H, s, C_{18}-CH_3), 0.85−2.28 (m), 2.43 (9 H, s, 3 × -N-CH_3), 2.76−2.92 (6 H, m, 3 × -N-CH_2), 3.22 (2 H, s, 1 × −CO-CH_2-N), 3.34 (2 H, m, 1 × −CO-CH_2-N), 3.40 (2 H, s, 1 × −CO-CH_2-N), 3.85- 3.93 (6 H, m, 3 × -O-CH_2-), 4.5−4.61 (1 H, m, C_3-CH), 4.95 (1 H, s, C_7-CH), 5.17 (1 H, s, C_{12}-CH), 6.46 (6 H, d, J = 8.0 Hz, 3 × Ar-CH), 6.72 (6 H, d, J = 8.0 Hz, 6 × −O-Ar-CH), 6.78−7.36 (30 H, m, 6 × C_6H_5). MS (ESI): m/z $(C_{107}H_{126}N_4O_{11})^+$ calcd, 1642.9; found, (M^+) 1642.3 (M^+).

Cell Culture. 4T1, MCF-7, T47D, and MDA-MB-231 cells were maintained as monolayers for experiments. 4T1 cells were cultured in RPMI-1640 media, and T47D, MCF-7, and MDA-MB-231 were cultured in DMEM (Hyclone, USA) containing 10% (w/v) fetal bovine serum, penicillin 100 μg/mL, streptomycin 100 U/mL, gentamycin 45 μg/mL at 37 °C in a humidified atmosphere with 5% CO_2. Subcultures were made by trypsinization and reseeded for experiments.

MTT Assay.[16] The cytotoxicity of tamoxifen and bile acid−tamoxifen conjugates (acids and amines) was estimated using the MTT {3-(4, 5-dimethylthiazol-2-yl)-2,5-diphenyltetrazolium bromide} assay. MTT was dissolved in PBS at a concentration of 5 mg/mL and filtered to sterilize. Approximately 3000−4000 cells/well were seeded in 96 well plates containing 200 μL of medium. After 24 h of preculture period to ensure attachment, the medium was removed. Fresh medium was added and supplemented with 1, 5, 10, 20, and 50 μM of tamoxifen (**Tam**) or tamoxifen equivalent concentrations of bile acid−tamoxifen conjugates (**LCA-Tam$_1$-Ad**, **DCA-Tam$_2$-Ad**, **CA-Tam$_3$-Ad**, **LCA-Tam$_1$-Am**, **DCA-Tam$_2$-Am**, and **CA-Tam$_3$-Am**). Cells were treated for 48 h with all of the compounds. After 48 h, 20 μL of MTT was added to each well and incubated for 4 h in an incubator, then a 1:1 mixture of DMSO and methanol was added. The optical density (OD) of each well was measured using a microculture plate reader with a test wavelength of 540 nm. The % viability was then calculated as $[\{A_{540}$ (treated cells) − background$]/[A_{540}$ (untreated cells) − background$\}]\cdot 100$.

Surface Plasmon Resonance Studies. Desired amount of DPPC was taken in round-bottomed wheaton glass vials in chloroform. Thin films were made under dry argon gas; and films were dried under vacuum for 6 h. Lipid films were hydrated with Milli Q water overnight. Hydrated films were then processed for 4−5 freeze thaw cycles from 70 to 4 °C with intermittent vortexing. Multilamellar vesicles were then sonicated at 70 °C for 15 min to get unilamellar vesicles.[17] All of the SPR experiments were performed on a Biacore T200 system equipped with an HPA sensor chip.[18] DPPC liposomes were prepared by the above-mentioned method with a final concentration of 2 mM. The running buffer was 1% DMSO containing Milli Q water. The analyte (drug) stocks were prepared in DMSO, and different concentrations were made such that the final concentration of DMSO in each was 1%. To mimic the *in vitro* experimental conditions, we performed the analysis at 37 °C maintaining the sample compartment at 42 °C. All of the required samples such as 2 mM liposomes, 40 mM octyl glucoside, 20 mM NaOH, and 0, 125, 250, 500 μM of analyte (**Tamoxifen**, **DCA-Tam$_2$-Ad**, **CA-Tam$_3$-Ad**, **LCA-Tam$_1$-Am**, **DCA-Tam$_2$-Am**, and **CA-Tam$_3$-Am**) were dispensed into single-use snap-capped vials, randomized in the rack base before they were ready for sample injection.

Liposome Immobilization and Analyte Binding Analysis. The new HPA chip was conditioned with two pulses of 40 mM octyl glucoside at a 10 μL/min flow rate for 100 s each, followed by washing the system with running buffer for 60 s. Then, 2 mM DPPC liposomes was injected at 5 μL/min flow rate for 500 s, followed by washing the system with running buffer for 100 s. Then, loosely bound or multilayered liposomes were washed away with two pulses of 20 mM NaOH injections at 30 μL/min flow rate for 45 s each. Finally, the HPA surface was washed for 100 s with running buffer at 30 μL/min flow rate to make the surface ready for drug binding analysis. Appropriate concentrations of analyte were placed in a rack and were allowed to be injected at a flow rate of 20 μL/min for 240 s of association and 150 s of dissociation. Finally, the surface was washed with running buffer for 100 s at 20 μL/min flow rate. To eliminate the carryover effect of analyte, the binding surfaces were completely washed away with 40 mM of octylglucoside, and a new lipid surface was prepared for each concentration of analyte being tested.

To minimize changes in the bulk refractive index between sample and running buffer, extreme care was taken to ensure that the drug and running buffers contained the same DMSO concentration. Data analyses were performed by subtracting an

average buffer response from all sample responses within each flow cell to eliminate artifacts that were flow cell dependent.

DPH Based Fluorescence Anisotropy. Fluorescence anisotropy studies were performed on unilamellar DPPC vesicles prepared by the above-mentioned method with preincorporation of DPH to make the final DPPC/DPH ratio 100:1. These liposomes were incubated with the required amount of bile acid−tamoxifen conjugates and **Tam** in 96-well plates at 37 °C up to 48 h. Steady state anisotropy measurements were done at different time points 6 h, 12 h, 24 h, and 48 h at 37 °C with these incubated samples using the fluorescence anisotropy protocol in a Molecular devices M5 instrument with λ_{ex} at 350 nm and λ_{em} of 452 nm. Steady state fluorescence anisotropy (r_s) was then calculated using the following equation:[19]

$$r_s = (I_{\parallel} - G \times I_{\perp})/(I_{\parallel} + 2 \times G \times I_{\perp})$$

where $I_{\parallel}$ and $I_{\perp}$ are the emission intensity excited with parallel-polarized light and measured with emission polarizer oriented in a parallel or perpendicular direction to the plane of excitation, respectively. G is an instrument specific factor calculated to correct the instrument polarization, which is equal to $I_{\perp\parallel}/I_{\perp\perp}$, and obtained by measuring the parallel and perpendicular polarized emission intensities after excitation with perpendicularly polarized light.

Annexin-FITC Analysis. The Annexin V-FITC (fluorescein isothiocyanate) labeled apoptosis detection kit (Sigma Chemical Co.) was used to detect and quantify apoptosis by flow cytometry as per the manufacturer's instructions. 4T1, MCF-7, T47D, and MDA-MB-231 cells (5×10^5 cells/well) were seeded onto each well in a 6-well plate. After 24 h, media were removed, and cells were treated with 10 μM of **Tam** or 10 μM tamoxifen equivalent conc of **CA-Tam$_3$-Am** for 48 h. After 48 h of treatment, cells were harvested in PBS and collected by centrifugation for 5 min at 2,000 rpm. Cells were then resuspended at a density of 1×10^6 cells/mL in 1× binding buffer and stained simultaneously with FITC labeled Annexin V (50 μg/mL) and propidium iodide (PI; 100 μg/mL) according to the manufacturer's protocol. Cells were analyzed using a flow cytometer (Becton Dickinson), and data were analyzed with Cell Quest software.

Cell Cycle Analysis. Cells were plated at a density of 2×10^5 cells per well for all cell lines in 6 well plates. After 24 h ensuring attachment of cells, media were removed, and fresh media were added to the cells. Cells were treated with 10 μM **Tam** or 10 μM tamoxifen equivalent conc of **CA-Tam$_3$-Am** for 48 h. After 48 h, cells were harvested using trypsin-EDTA and washed twice with 1× ice cold PBS and fixed in 70% ethanol at 4 °C. Cells were washed again with PBS at least 2 times to remove all of the ethanol. Ten microliters of RNase (20 mg/mL) was added, and cells were kept at 37 °C for 1 h. The cells were stained at room temperature for 20 min in 50 μg/mL propidium iodide. The cells were then counted on a FACS (Becton Dickinson, Mountain View, CA), and percentages of cells in G1, S, and G2/M phases of the cell cycle were determined using ModFit LT software (Verity Software House, Topsham, ME).

ROS Generation. Intracellular ROS levels were measured using dichlorodihydrofluorescein diacetate (DCFDA, Sigma Chemicals Co.). DCFDA is an uncharged nonfluorescent cell-permeable compound. After entering inside the cells, the diacetate bond is cleaved by nonspecific esterases to form polar and nonfluorescent DCFDA. The generation of ROS oxidizes DCFDA and coverts it to DF that yields green fluorescence. 4T1, MCF-7, T47D, and MDA-MB-231 cells (20,000 cells/well) were seeded in 96 black well plates and grown for 24 h. After 24 h, cells were washed thrice with DPBS containing 0.2% FBS, and 25 μM of DCFDA in DPBS containing 0.2% FBS was added for 30 min at 37 °C, followed by the addition of **Tam** and **CA-Tam$_3$-Am** at 10 μM tamoxifen equivalent concentration. Nontreated cells served as controls, and these cultures received equivalent volumes of the DMSO solvent. Fluorescence emission was recorded using a 96 well plate reader (Spectramax pro 5) using excitation and emission wavelengths of 485 and 535 nm up to 1 h at the intervals of 15 min. The experiments were repeated at least three times.

Real Time PCR Studies. mRNA expression levels of pro-apoptotic, antiapoptotic, and caspases (BCl-2, Bcl-X$_L$, BAX, Bid, Bad, caspase 8, caspase 3, caspase 9, survivin, and cytochrome *c*) were analyzed by quantitative real time reverse transcription-PCR based on SYBR Green Chemistry using GAPDH as internal reference. SYBR Green Universal Master-Mix was obtained from Applied Biosystems GmbH (Weiterstadt, Germany). Total cellular RNA was isolated from MCF-7 and MDA-MB-231 cells using RNeasy kit (Qiagen). One microgram of RNA was used for *c*DNA synthesis by using the First Strand cDNA Synthesis kit (Applied Biosystems). The PCR was done in 96 well microtiter plates in an ABI Fast 7500 Detection System (Applied Biosystems). The reaction mixture consisted of 5 μL of SYBR Green Master Mix, 0.5 μL of forward and reverse primer each, and equal amounts of cDNA as template from control as well as treated cells. Cycling conditions for the reaction are as follows: initial denaturation of template DNA and activation of enzyme for 95 °C for 5 min, 40 cycles consisting of denaturation at 95 °C for 45 s, and annealing/extension at 55 °C for 1 min. Each sample was tested in triplicate. The relative expression of each gene was determined on the basis of threshold cycle (C_T value). Quantity of cDNA was normalized in reference to the GAPDH gene that is used as the internal control. Then, normalized target gene expression was divided by the normalized gene expression value of untreated control cells to obtain the fold change of gene after treatment. The SD of normalized target gene expression relative to GAPDH is calculated from initial SDs of target gene and GAPDH. The primer pairs used in this study for PCR amplification are Bcl-2 (forward, GGATTGTGGCCTTCTTTGAG; reverse, CCAAACTGAGCAGAGTCTTC), Bcl-X$_L$ (forward, ATGAACTCTTCCGGGATGG; reverse, TGGATCCAAGGCTCTAGGTG), Bax (forward, TTTGCTTCAGGGTTTCATCC; reverse, GCCACTCGGAAAAAGACCTC), Bid (forward, ACAGCATGGACCGTAGCATC; reverse, GTGTGACTGGCCACCTTCTT), Bad (forward, AGTCGCCACAGCTCCTACC; reverse, GGCGAGGAAGTCCCTTCTTA), Survivin (forward, AGAACTGGCCCTTCTTGGAGG; reverse, CTTTTTATGTTCCTCTATGGGGTC); cyt *c* (forward, TGGACCACTCCATTGCCATC; reverse, AGACAGGACACTGCGGAAAG), caspase 8 (forward, CATCCAGTCACTTTGCCAGA; reverse, GCATCTGTTTCCCCATGTTT), caspase 3 (forward, TGGAATTGATGCGTGATGTT; reverse, GGCAGGCCTGAATAATGAAA) caspase 9 (forward, TGACTGCCAAGAAAATGGTG; reverse, CAGCTGGTCCCATTGAAGAT), GAPDH (forward, CACCATCTTCCAGGAGCGAG; reverse, TCACGCCACAGTTTCCCGGA).

Western Studies. Total proteins were extracted from approximately 1×10^7 MCF-7 and MDA-MB-231 cells treated

Table 1. IC_{50} (μM) Values of Tam and Bile Acid−Tamoxifen Conjugates with Respect to Tamoxifen Equivalent Concentrations in Different ER +ve and ER −ve Cancer Cell Lines

	4T1	MCF-7	T47D	MDA-MB 231
Tam	12.25 ± 1.92	18.25 ± 4.19	22.41 ± 2.15	19.41 ± 4.47
LA-Tam$_1$-Ad	19.49 ± 4.62	41.65 ± 2.58	45.71 ± 2.91	33.97 ± 1.96
DCA-Tam$_2$-Ad	18.17 ± 1.14	37.77 ± 3.19	>50	35.74 ± 3.61
CA-Tam$_3$ -Ad	20.28 ± 3.88	49.33 ± 7.06	>50	27.0 ± 4.15
LA-Tam$_1$-Am	19.23 ± 0.71	46.96 ± 5.12	49.95 ± 6.19	41.48 ± 4.48
DCA-Tam$_2$-Am	22.05 ± 4.13	41.75 ± 4.11	49.17 ± 4.98	35.21 ± 4.46
CA-Tam$_3$-Am	5.28 ± 4.32	8.1 ± 3.82	9.42 ± 4.21	17.55 ± 5.85

with **Tam** and **CA-Tam$_3$-Am** at 10 μM tamoxifen equivalent concentration for up to 48 h. Cells were washed with ice-cold PBS and lysed in RIPA buffer (50 mM Tris-Cl, pH 8.0, 150 mM NaCl, 1% NP-40, 0.5% sodium deoxycholate, 2 mM EDTA, 1 mM PMSF, NaF, and protease inhibitor cocktail from Sigma Aldrich) for 30 min at 4 °C. Insoluble material was removed by centrifugation at 12,000*g* for 15 min at 4 °C. Equal amounts of proteins were loaded under denaturing conditions on 10 and 12% SDS−polyacrylamide gels and transferred to the nitrocellulose membrane (MDI, Ambala, India). Membranes were blocked with 5% nonfat milk in PBST. The membranes were probed with specific antibody (Cell Signaling Technologies, NEB, Frankfurt, Germany) for 2 h at room temperature or overnight at 4 °C, followed by washing in PBS containing 0.5% Tween-20. Thereafter, the blot was incubated in peroxidase-conjugated secondary antibody of 1:5000 dilution. Blots were reprobed with β-actin antibody (Sigma) as an internal control. Secondary anti-Rabbit HRP conjugated antibody was used for all of the antibodies used except for β-actin where anti-mouse secondary HRP conjugated antibody was used. The results were analyzed and documented using GE image quant and documentation software (Image Quant LAS 4000).

In Vivo 4T1 Tumor Model in Balb/c Mice. The murine 4T1 breast cancer cells (1.5×10^7) were implanted subcutaneously in the right flanks of 4−6 week-old female Balb/c mice. After tumor sizes reached around 150 mm^3, animals were administered with intratumor injections of DMSO vehicle control (100 μL), tamoxifen (15 mg/kg dissolved in 100 μL of DMSO), and **CA-Tam$_3$-Am** (15 mg/kg tamoxifen equivalent dose dissolved in 100 μL of DMSO) once a week. Treatment was started on day 7 postimplantation and again administered once on day 13 (weekly dosage). The tumor volumes were monitored on alternate days. The tumor volume was calculated by using the formula, $w^2 \times 1/2$. All animal procedures were approved by the Institutional Animal Ethical Committee (IAEC), NII.

Statistical Analysis. All statistical analyses were performed using GraphPad Prism, version 5 (GraphPad Software Inc., San Diego, CA, USA). The results of flow cytometry and qRT-PCR are presented as mean ± SD. Densitometry was performed using ImageJ software. The intensities of the protein or mRNA bands were normalized to actin bands and quantified by comparing with those of control cells.

RESULTS AND DISCUSSION

Chemistry. We synthesized two series comprising six bile acid−tamoxifen conjugates based on three bile acids lithocholic acid (**LCA**), deoxycholic acid (**DCA**), and cholic acid (**CA**). These two series of bile acid−tamoxifen conjugates are based on having acid functionality or amine functionality free at the tail region of bile acids (Figure 1). As tamoxifen does not have any active functional group for conjugation, we first synthesized *N*-desmethylated tamoxifen from tamoxifen by reacting with 2-chloroethyl chloroformate.[20] Bile acid−tamoxifen conjugates bearing acid functionality were synthesized (Scheme 1) from corresponding bile acids (**LCA**, **7a**; **DCA**, **7b**; **CA**, **7c**) first by protection of acid functional groups as methyl esters in the presence of conc HCl in excess methanol at room temperature for 12 h with 98% yield. Methyl ester derivatives of bile acids (**8a**, **8b**, and **8c**) were reacted with chloroacetic anhydride in the presence of pyridine and a catalytic amount of DMAP in toluene at 90 °C overnight. Chloroacetoxy derivatives (**9a**, **9b**, and **9c**) were obtained in 80−88% yield after purification by flash chromatography. Tamoxifen was conjugated to chloroacetoxy derivatives of bile acids using *N*-desmethylated tamoxifen. Chloroacetoxy derivatives were refluxed with *N*-desmethylated tamoxifen in anhydrous acetonitrile for 16 h to give compounds **10a**/**10b**/**10c** with 65−70% yield. Final bile acid−tamoxifen conjugates having acid functional groups were synthesized by controlled basic hydrolysis of **10a**/**10b**/**10c** at lower temperature, as ester linkages between bile acids and tamoxifen are sensitive to this basic hydrolysis. Hydrolysis of methyl esters was performed with 2 N NaOH at 0 °C, followed by stirring at room temperature for 6 h to get the final compounds (**1**, **2**, and **3**) in 40−48% yield.

For the synthesis of bile acid−tamoxifen conjugates bearing amine groups (Scheme 2), bile acids were first derivatized to *N*-boc-ethanolamine derivatives (**11a**/**11b**/**11c**). Bile acids were activated with *N*-hydroxysuccinamide and EDC·HCl at room temperature for 8 h. Activated bile acids were reacted with boc-ethanolamine in DMF at room temperature for overnight to get boc-ethanolamine derivatives in 80−85% yield. Boc-ethanolamine derivatives of bile acids were then reacted with chloroacetic anhydride in toluene in the presence of pyridine and DMAP. The reaction mixture was heated at 90 °C for 12 h to get chloroacetoxy derivatives (**12a**, **12b**, and **12c**) in 75−90% yields. Tamoxifen was conjugated to these chloroacetoxy derivatives by refluxing the reaction mixture of chloroacetoxy derivative, *N*-desmethylated tamoxifen, and triethylamine in acetonitrile for 16 h to get tamoxifen conjugated derivatives (**13a**, **13b**, and **13c**) in 70−80% yield. Boc protection was removed from these bile acid−tamoxifen conjugates using trifluoroacetic acid (TFA) in dichloromethane at 0 °C and further stirring the reaction mixture at room temperature for 6 h. The amine derivative of bile acid−tamoxifen conjugates was purified by precipitation in a hexane−ether mixture to give a colorless solid in quantitative yields. To get final compounds (**4**, **5**, and **6**), chloride anion exchange was performed with TFA derivatives of tamoxifen−bile acid conjugates using amberlyte IRA-900 by stirring the reaction mixture at room temperature for 8 h followed by filtration. All intermediates and final

compounds were characterized by ^{1}H NMR and mass spectral studies.

***In Vitro* Anticancer Activities (MTT Assay).** We studied the anticancer activities of bile acid−tamoxifen conjugates along with the prototype drug tamoxifen in three estrogen receptor +ve breast cancer cell lines, 4T1, MCF-7, and T47D, and in one estrogen receptor −ve breast cancer cell line, MDA-MB-231, at different tamoxifen equivalent concentrations of 1, 5, 10, 20, and 50 μM for 48 h. Tamoxifen has shown 50% cytotoxicity at 10−25 μM in four breast cancer cell lines (Figure S1, Supporting Information), and interestingly, tamoxifen IC_{50} values were similar in both ER +ve and ER −ve cell lines (Table 1). These results clearly indicate that tamoxifen operates via multiple mechanisms of action to bring cytotoxicity in breast cancer cells, and to show effectiveness by a nonclassical mechanism, tamoxifen requires a dose similar to that needed for the classical ER mechanism.[21] Nonclassical mechanisms include the interaction of tamoxifen with hydrophobic regions of membrane lipids influencing fluidic states of the membrane and inhibiting enzymes involved in cellular proliferation by putative interactions with phospholipids. [22] Bile acid−tamoxifen conjugates with acid head groups (**LCA-Tam$_1$-Ad**, **DCA-Tam$_2$-Ad**, and **CA-Tam$_3$-Ad**) showed 50% cell death at high concentrations (Figure S1, Supporting Information) with a broad range between 17 and >50 μM (Table 1). Low efficacy of bile acid−tamoxifen conjugates having acid groups may be due to reversible interactions between these conjugates and the cell membrane and therefore the lack of penetration of these conjugates through the cell membrane leading to low intracellular accumulation of tamoxifen inside the cells. However, among bile acid−tamoxifen conjugates with amine head groups (Figure S2, Supporting Information), **LCA-Tam$_1$-Am** and **DCA-Tam$_2$-Am** have shown similar cellular toxicities with high IC_{50} values (Table 1). **LCA-Tam$_1$-Am** and **DCA-Tam$_2$-Am** may show strong interactions with cell membranes, but these strong interactions may not be enough for high penetration of these conjugates in cell membranes as explained later in SPR and fluidity studies. Cholic acid based **CA-Tam$_3$-Am** possessing three tamoxifen molecules and amine functionality was found to be most potent and showed IC_{50} at ∼5 μM, ∼8 μM, and ∼9 μM w.r.t. tamoxifen in ER +ve cell lines 4T1, MCF-7, and T47D, respectively, and it is 2- to 3-fold more effective than tamoxifen. In ER −ve cell lines (MDA-MB-231), **CA-Tam$_3$-Am** showed anticancer activities similar to those of tamoxifen. Conjugation of three tamoxifen molecules to cholic acid having an amine group, **CA-Tam$_3$-Am**, could increase intracellular accumulation of tamoxifen that is responsible for the high efficacy of **CA-Tam$_3$-Am**. The 2- to 3-fold differences in IC_{50} values of **CA-Tam$_3$-Am** in ER +ve and ER −ve cell lines may be due to classical and nonclassical anticancer mechanisms of **CA-Tam$_3$-Am** in ER +ve and ER −ve cell lines, respectively. The nonclassical mechanism of **CA-Tam$_3$-Am** may be due to the effective intercalation of large, extended hydrophobic aromatic groups of **CA-Tam$_3$-Am** with hydrophobic regions of membrane lipids.

MTT results showed that anticancer activities of bile acid−tamoxifen conjugates with acid and amine head groups strongly depend on surface charge and number and positional grafting of tamoxifen molecules to bile acids. Anticancer activities in ER +ve and ER −ve cell lines indicate the existence of multiple cellular actions of these conjugates at different levels. The high potential activity of **CA-Tam$_3$-Am** may be due to the effective interactions of **CA-Tam$_3$-Am** with membrane lipids and more accumulation of tamoxifen molecules inside cancer cells. We then compared the toxicity of **CA-Tam$_3$-Am** with the control where cells were treated with a physical mixture containing one equivalent of amine-modified cholic acid and 3 equivalents of tamoxifen (**CA-Am**:**Tam** = 1:3) (Figure S3, Supporting Information). We have observed that **CA-Tam$_3$-Am** is more toxic in ER +ve MCF-7 than in a physical mixture of **CA-Am**:**Tam**, whereas we observed a similar toxicity profile in the ER −ve MDA-MB-231 cell line.

To explore the differential anticancer activities of bile acid−tamoxifen conjugates and to decipher the role of charge and hydrophobicity on membrane interactions, we studied the interactions of bile acid−tamoxifen conjugates with model DPPC membranes on incubation of these lipid drug conjugates with DPPC liposomes using surface plasmon resonance (SPR) and DPH anisotropy based membrane fluidity studies.

Surface Plasmon Resonance (SPR) Studies. One of the major barriers for drug delivery is the cell membrane that regulates not only the transport of essential nutrients, ions, and exogenous materials but also regulates the passage of xenobiotics such as drugs.[23] Irreversible drug−membrane interactions are crucial for the effective binding of drugs to the membrane, its penetration through the lipid bilayer of cell membranes, its bioactivity, and intracellular actions that dictate the intracellular fate of the drug, whereas reversible interactions would not allow the penetration of the drug molecules inside the cells leading to less intratumor uptake. Drug−membrane interactions can be studied using biosensor based techniques to predict their pharmacokinetic properties such as mechanisms of transport (passive/active), distribution, and accumulation that strongly depend on the physicochemical properties of drugs.[24]

SPR is a well established and powerful optical biosensor technique in real-time monitoring of bio molecular interactions with other biomolecules as well as small molecules. Over the past decade, the SPR technique was well explored in the pharmaceutical field to study drug−receptor interactions,[25,26] pharmacokinetic profiles such as bioavailability,[27] and plasma protein binding[28] that has proved to reduce research cost effects in preclinical development of leads and their modifications. Physico-chemical events in drug binding to lipid surfaces involves electrostatic interactions of drug molecules with polar phosphate component of lipids followed by interaction of the drugs' hydrophobic part with lipophilic acyl chains of lipids that are critical factors as it controls the passive entry of drug molecules into the intracellular compartment.[29] These electrostatic interactions are crucial to the initial entry of drugs when crossing the cell membrane barrier.[30] Hydrophobic interactions between the drug and the lipid alkyl chain is a low affinity and high capacity process,[31] and the extent of these interactions dictates the drug's activity inside the cells.

Therefore, to understand the differential *in vitro* anticancer activities of bile acid−tamoxifen conjugates, we explored the binding studies of bile acid−tamoxifen conjugates with model DPPC membranes. Analysis of sensograms (Figure S4, Supporting Information) showed that free **Tam** and all bile acid−tamoxifen conjugates showed dose dependent increase in binding responses with lipid surfaces in association and in dissociation phases. Tamoxifen showed an initial bulk response followed by binding type association phase, and at higher concentrations, it showed the formation of stable tamoxifen−lipid complexes where tamoxifen is intercalated in the alkyl chains of DPPC lipids. Bile acid−tamoxifen conjugates bearing

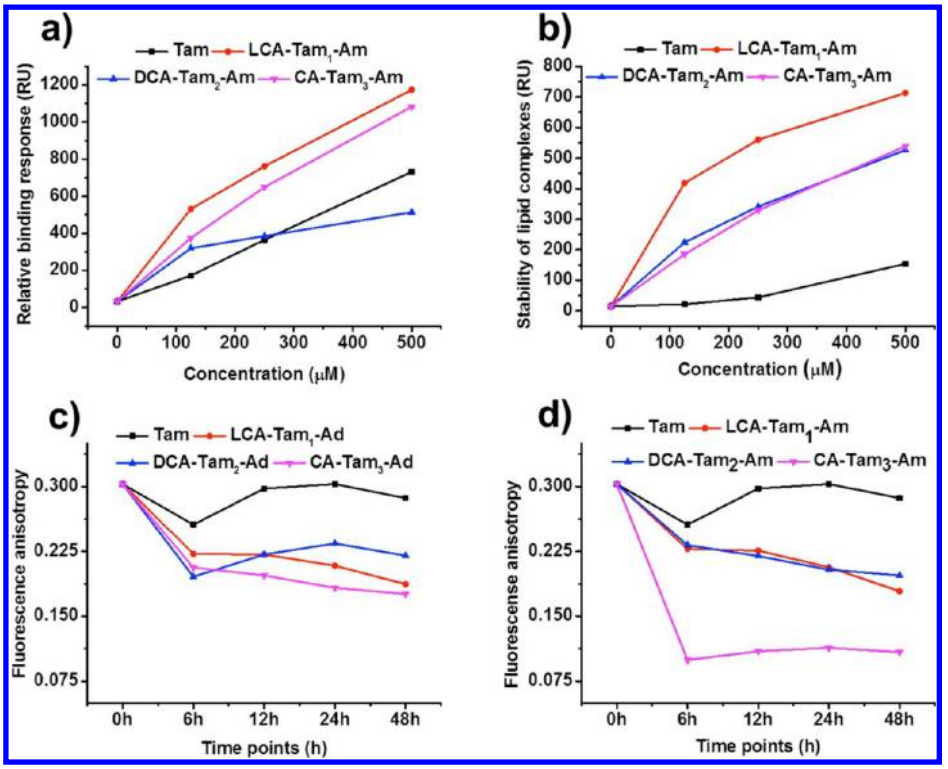

Figure 2. (a, b) SPR studies: concentration dependent (a) drug binding responses and (b) stable drug–lipid complex responses formed by irreversible binding of bile acid–tamoxifen conjugates with amine head groups and **Tam**. (c, d) DPH anisotropy studies: time dependent changes in DPH anisotropy (membrane rigidity/fluidity) of DPPC membranes by incubation of **Tam** and bile acid–tamoxifen conjugates at 37 °C. (c) Bile acid–tamoxifen conjugates with acid head groups; (d) bile acid–tamoxifen conjugates bearing amine head groups.

acid head groups (**DCA-Tam$_2$-Ad** and **CA-Tam$_3$-Ad**) show high bulk response as compared to tamoxifen in the association phase followed by a steep decrease in RU (Response Units) in the dissociation phase indicating its reversible mode of binding with the lipid surface (Figures S4b and c, Supporting Information), whereas we could not perform the SPR studies with **LCA-Tam$_1$-Ad** due to its solubility problems in different running buffer conditions. The reversible binding nature of bile acid–tamoxifen conjugates having acid headgroups (**DCA-Tam$_2$-Ad** and **CA-Tam$_3$-Ad**) to model membranes (Figure S4b and c, Supporting Information) is evident from our *in vitro* anticancer data (Figure S1, Supporting Information) that show the low activity of these conjugates in four breast cancer cell lines, as bile acid–tamoxifen conjugates bearing acid groups do not form stable bonds with the cell membrane surface.

However, bile acid–tamoxifen conjugates with amine head groups showed high bulk response in RU followed by association binding with the lipid surface leading to stable modes of binding (Figure S4d, e, and f, Supporting Information). **LCA-Tam$_1$-Am** was found to form stable complexes with the lipid membrane even after washing with running buffer. **CA-Tam$_3$-Am** binds to the lipid membrane as efficiently as **LCA-Tam$_1$-Am**, but after washing with running buffer, it showed the inferior stability of intercalated complexes compared to **LCA-Tam$_1$-Am**. **DCA-Tam$_2$-Am** showed inferior binding compared to that of **CA-Tam$_3$-Am** and **LCA-Tam$_1$-Am** in association phase, but the stability of lipid complexes formed with **DCA-Tam$_2$-Am** is similar to that of **CA-Tam$_3$-Am** (Figure 2). The order of binding responses of these bile acid–tamoxifen conjugates to the lipid surface is **LCA-Tam$_1$-Am** ≈ **CA-Tam$_3$-Am** > **Tamoxifen** > **DCA-Tam$_2$-Am** (Figure 2a), whereas the order of forming stable intercalated complexes with the lipid surface is **LCA-Tam$_1$-Am** > **CA-Tam$_3$-Am** = **DCA-Tam$_2$-Am** > tamoxifen (Figure 2b).

SPR studies conclude that the presence of acid head groups on bile acid–tamoxifen conjugates showed a reversible binding response with membranes due to the lack of essential electrostatic interactions with phospholipids leading to low penetration of these conjugates and therefore low anticancer activities. Amine derivatives of bile acid–tamoxifen conjugates showed stable binding to membrane surfaces indicating that the presence of an amine headgroup is essential for effective electrostatic interactions of these molecules with polar phosphocholine head groups of membranes. The extent of drug–lipid surface interactions measured by SPR showed a strong +ve correlation with *in vitro* cytotoxicity studies showing that acid derivatives of bile acid–tamoxifen conjugates are less effective. Once the molecules establish effective electrostatic interactions with membranes, the next step involves the hydrophobic interactions of lipid–drug conjugates with the cellular lipid bilayer in a process of passive transport, which is the next barrier for the effective delivery of drugs.[32] As these molecules having large hydrophobic surfaces form stable complexes with the lipid bilayer, we studied the interactions of these molecules in the induction of fluidity/rigidity in membranes by DPH based fluorescence anisotropy. These studies can also allow us to explore the differential activities of amine derivatives of bile acid–tamoxifen conjugates.

DPH Based Fluorescence Anisotropy Studies. Induction of fluidity in the membrane by drug molecules is one of the important factors for multiple mechanisms of action of drugs.[33] We explored the changes in rigidity/fluidity in ordered regions of membranes induced by stable lipid–drug complexes of these bile acid–tamoxifen conjugates to understand their differences

dx.doi.org/10.1021/bc300664k | *Bioconjugate Chem.* 2013, 24, 1468–1484

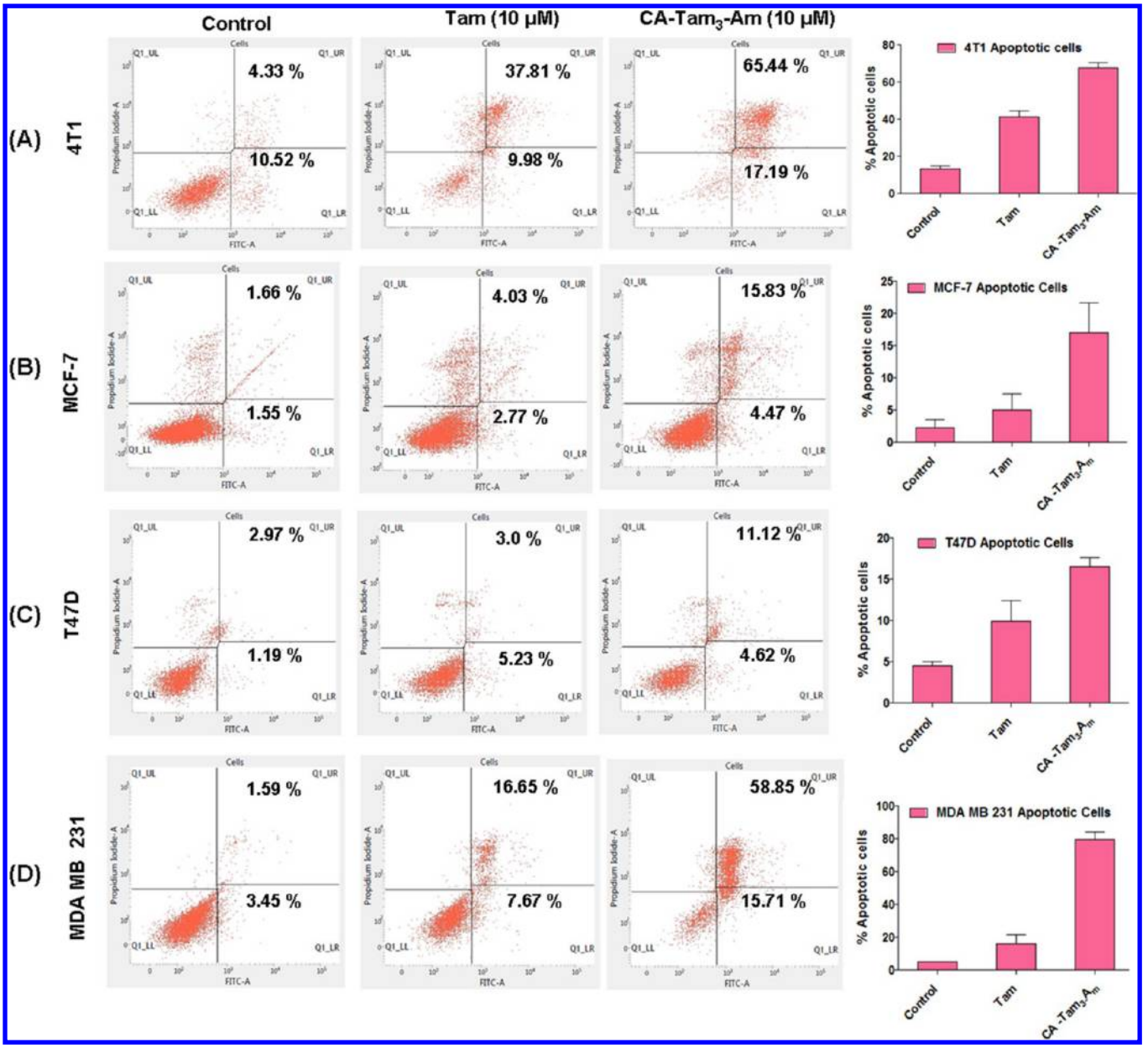

Figure 3. Annexin-V/FITC apoptosis assay in (A) 4T1, (B) MCF-7, (C) T47D, and (D) MDA-MB 231 cells treated with Tamoxifen (**Tam**) and **CA-Tam$_3$-Am** at 10 μM tamoxifen equivalent concentration for 48 h.

in *in vitro* activities.[34] Influence of drugs on membrane fluidity can be studied using fluorescence anisotropy studies using diphenylhexatriene (DPH) as a probe. DPH having a hydrophobic nature interacts with hydrophobic alkyl chains of membrane lipids. The rotational motions of this fluorophore (DPH) are restricted by alkyl chains in ordered gel phase that lead to high anisotropy values. Drug molecules that induce fluidity in gel phase by disrupting alkyl chain regions will have an impact on the rotational motions of DPH, and hence, we would expect more fluidity and lower anisotropy values.

We mimic the *in vitro* cell culture conditions and incubated DPH doped DPPC liposomes with free tamoxifen and bile acid−tamoxifen conjugates at 37 °C for 48 h. Incubation of tamoxifen and bile acid−tamoxifen conjugates decreases the membrane anisotropy in a time dependent manner making the membranes more fluidic, but the extent of fluidity change depends on bile acid, the charge on bile acids, and the number of tamoxifen molecules conjugated (Figure 2c,d). Bile acid tamoxifen conjugates with acid and amine functionalities have shown greater membrane fluidity compared to that of free tamoxifen. Incubation of tamoxifen causes maximum fluidity within 6 h of incubation (Figure 2c), and subsequent increase in fluorescence anisotropy values may be due to the equilibrium shift between incubated molecules and DPPC membranes. All bile acid−tamoxifen conjugates having acid functionality (**LCA-Tam$_1$-Ad**, **DCA-Tam$_2$-Ad**, and **CA-Tam$_3$-Ad**) increase the membrane fluidity only to a minor extent at physiological temperature (37 °C), which is also evident from SPR studies that showed reversible binding interactions between acid conjugates and membranes. Therefore, the ineffectiveness of these bile acid−tamoxifen conjugates with acid functionalities is due to (1) the lack of favorable (irreversible) interactions with polar regions of membranes and (2) the low intercalation of these derivatives in membranes changing membrane fluidity.

dx.doi.org/10.1021/bc300664k | *Bioconjugate Chem.* 2013, 24, 1468−1484

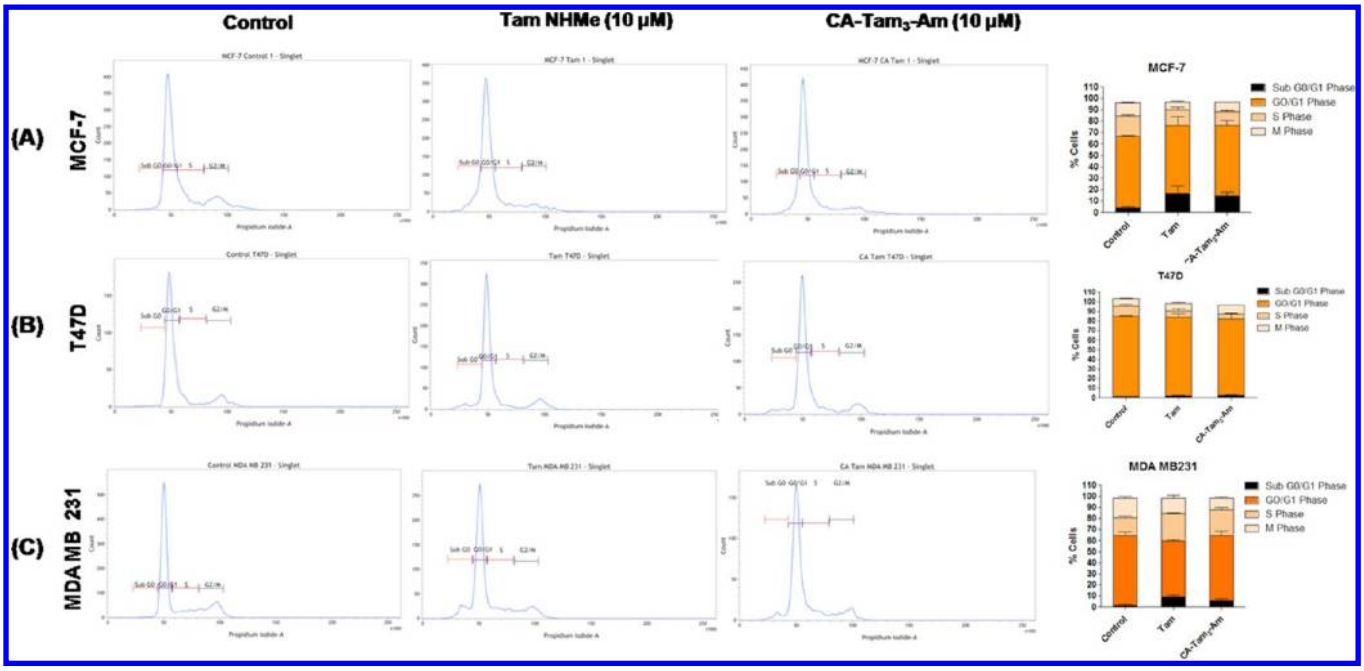

Figure 4. Cell cycle analysis in (A) MCF-7, (B) T47D, and (C) MDA-MB 231 cells treated with Tamoxifen (**Tam**) and **CA-Tam$_3$-Am** at 10 μM tamoxifen equivalent concentration for 48 h.

Among amine derivatives of bile acid−tamoxifen conjugates, **LCA-Tam$_1$-Am** and **DCA-Tam$_2$-Am** cause less changes in membrane fluidity at 37 °C (Figure 2d) like bile acid−tamoxifen conjugates with acid functionalities; whereas incubation of **CA-Tam$_3$-Am** caused maximum distortions in membrane packing leading to a decrease in fluorescence anisotropy indicating higher fluidity changes in membranes.[35] Incubation of membranes with **CA-Tam$_3$-Am** for 24 h causes a 3-fold increase in membrane fluidity than tamoxifen and a 2-fold increase than **LCA-Tam$_1$-Am** and **DCA-Tam$_2$-Am**. **CA-Tam$_3$-Am** with its large aromatic hydrophobic surface can intercalate with hydrophobic alkyl chains of lipids and cause maximum distortions leading to high membrane fluidity and penetration. The order of membrane fluidity induced by bile acid−tamoxifen conjugates on incubation with DPPC membranes for 48 h at 37 °C is **CA-Tam$_3$-Am** > **LCA-Tam$_1$-Am** > **DCA-Tam$_2$-Am** > tamoxifen.

A comparison of cytotoxicity, SPR, and membrane fluidity studies showed that bile acid−tamoxifen conjugates having acid head groups fail to establish effective electrostatic interactions with membranes due to reversible binding (from SPR studies), and hence they are unable to intercalate in the membranes causing less membrane fluidic changes (from DPH studies). This reversible binding and low penetration result in lower *in vitro* anticancer activities (MTT assay) of these conjugates (Table 1). However, bile acid−tamoxifen conjugates having amine head groups show effective (irreversible) binding with membranes forming stable lipid−drug complexes (SPR studies), and their intercalation in membranes strongly depends on the number and position of tamoxifen molecules conjugated to bile acid. Among bile acid−tamoxifen conjugates with amine head groups that bind and form stable drug−lipid complexes, **CA-Tam$_3$-Am** causes more fluidic changes in DPPC membranes making it most potent. We then explored the intracellular apoptotic mechanism of **CA-Tam$_3$-Am** and compared it with tamoxifen using Annexin-FITC, cell cycle, ROS, PCR, and Western studies.

Apoptotic Studies Using Annexin-FITC and Cell Cycle Analysis. To explore the mechanism of cell death by **CA-Tam$_3$-Am**, we probed **Tam** and the cholic acid−tamoxifen conjugate (**CA-Tam$_3$-Am**) treated (10 μM tamoxifen equivalent conc) cancer cells with an Annexin-V-FITC labeled apoptosis detection kit (Sigma Chemical Co.) As shown in Figure 3, treatment of **Tam** led to the progression of 6.7%, 8.2%, 47%, and 24% of Annexin- and PI +ve cells in MCF-7, T47D, 4T1, and MDA-MB-231, respectively, whereas **CA-Tam$_3$-Am** treatment led to the progression of 20%, 15.7%, 82%, and 74% Annexin- and PI +ve cells in MCF-7, T47D, 4T1, and MDA-MB-231, respectively. These results indicate that treatment with **CA-Tam$_3$-Am** causes a 2−3-fold increase in the number of total apoptotic (early and late) cells. We have observed a 2-fold increase in apoptotic cells in ER +ve cell lines MCF-7, T47D, and 4T1 and a 3-fold increase in ER −ve MDA-MB-231 cells upon treatment of **CA-Tam$_3$-Am** as compared to tamoxifen. These results show that conjugation of tamoxifen with bile acid has increased the availability of tamoxifen to cancer cells irrespective of ER status and even found to be more effective for estrogen receptor −ve cells like MDA-MB-231.

We then explored the fate of cells in different phases of the cell cycle by propidium iodide based cell cycle analysis in three cell lines upon treatment of tamoxifen and **CA-Tam$_3$-Am** at 10 μM for 48 h as shown in Figure 4. Cell cycle analysis showed that treatment of tamoxifen and **CA-Tam$_3$-Am** in breast cancer cell lines causes sub-G_0 cell cycle arrest that is in agreement with the earlier reports.[36]

Generation of Reactive Oxygen Species (ROS). Reactive oxygen species (ROS) and mitochondria play an important role in apoptosis induction under both physiologic and pathologic conditions.[37] Interestingly, mitochondria are both the source and target of ROS,[38] and cytochrome *c* release from mitochondria, which triggers caspase activation, appears to be largely mediated by the direct or indirect action of ROS. To study the effect of tamoxifen and **CA-Tam$_3$-Am** on intracellular ROS levels of T47D, MCF-7, 4T1, and MDA-

dx.doi.org/10.1021/bc300664k | *Bioconjugate Chem.* 2013, 24, 1468−1484

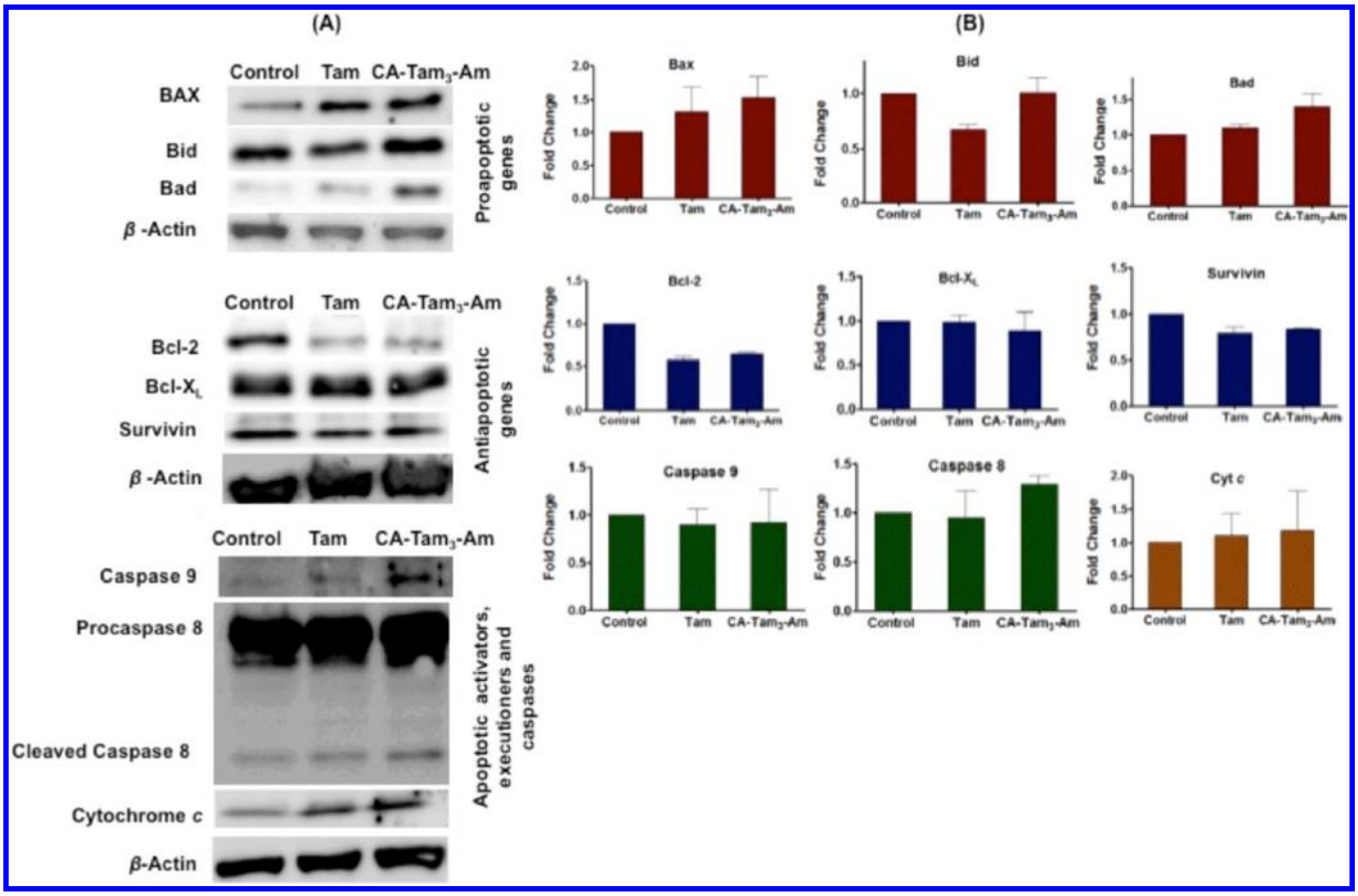

Figure 5. (A) Western Blot studies of MCF-7 cells treated with **Tam** and **CA-Tam$_3$-Am** at 10 μM tamoxifen equivalent concentration for 48 h. (B) Graphical representation of densitometry of all proteins in the Western blot performed in triplicate with ± SD. All of the values were normalized using β-actin as the internal control.

MB-231 cells, cells loaded with DCFDA were treated with tamoxifen and **CA-Tam$_3$-Am**. After treatment, the measurement of ROS production was monitored up to 60 at 15 min interval. We observed time and dose dependent rapid and robust increase in ROS levels, which have been quantified as fluorescence units as shown in (Figure S5, Supporting Information). There is not much alteration in levels of ROS production in T47D cells, whereas the ROS levels measured were approximately 1.2-fold and 2-fold in MCF-7 cells incubated with tamoxifen and **CA-Tam$_3$-Am**, respectively. Similarly there is 1.1- and 1.4-fold increase in ROS levels after treatment with tamoxifen and **CA-Tam$_3$-Am** in 4T1 cells. MDA-MB-231 cells show 1.1- and 1.4-fold increase in ROS levels for tamoxifen and **CA-Tam$_3$-Am**, respectively. Quantification of ROS levels measured by fluorescence units showed high levels of ROS generation in ER −ve cell lines (MDA-MB-231) as compared to ER +ve cell lines (4T1, T47D, and MCF-7).

The generation of ROS in MCF-7 and MDA-MB-231 cell lines indicate that these cells undergo intrinsic pathway of apoptosis as both of the cell lines show high expression of cytochrome *c* (as described later). Generation of ROS is much higher in response to **CA-Tam$_3$-Am** treatment as compared to that to tamoxifen. Increased levels of ROS upon treatment with **CA-Tam$_3$-Am** may be due to the higher permeability of cells to **CA-Tam$_3$-Am** resulting in the generation of a higher amount of ROS inside mitochondria and making the mitochondrial membrane more permeable, releasing cytochrome *c* that further activates regulatory machinery of the cells toward apoptosis.

Regulation of Antiapoptotic and Pro-Apoptotic Genes. The induction of apoptosis in ER +ve and ER −ve cells may be a result of the sequence of genes triggered in response to chemical stimuli. Apoptosis can be triggered by two mechanisms either by the activation of an intrinsic pathway that includes proteins from the Bcl-2 family or by an extrinsic pathway that involves death receptors on the cell surface.[39] Apoptosis using the intrinsic pathway induces mitochondrial membrane permeation and increase in levels of cytochrome *c* in the cytoplasm. Induction of this pathway leads to a downstream cascade of events, releasing various apoptotic mediators from mitochondria[40] and activation of caspases that are important for the fate of the cell.

Commitment of cells to apoptosis is governed largely by protein−protein interactions between members of the Bcl-2 family. These are key regulators of apoptosis that include both anti- and proapoptotic genes. In normal conditions, there is always a dynamic balance between pro- and antiapoptotic proteins, and a slight change in the dynamic balance of these proteins may result either in inhibition or induction of cell death. Therefore, we studied the influence of tamoxifen and **CA-Tam$_3$-Am** on the expression of mRNA and protein levels encoding proapoptotic and antiapoptotic members of the Bcl-2 family along with caspase activators and executioners in MCF-7 (ER +ve) and MDA-MB-231 (ER −ve) cells.

dx.doi.org/10.1021/bc300664k | *Bioconjugate Chem.* 2013, 24, 1468−1484

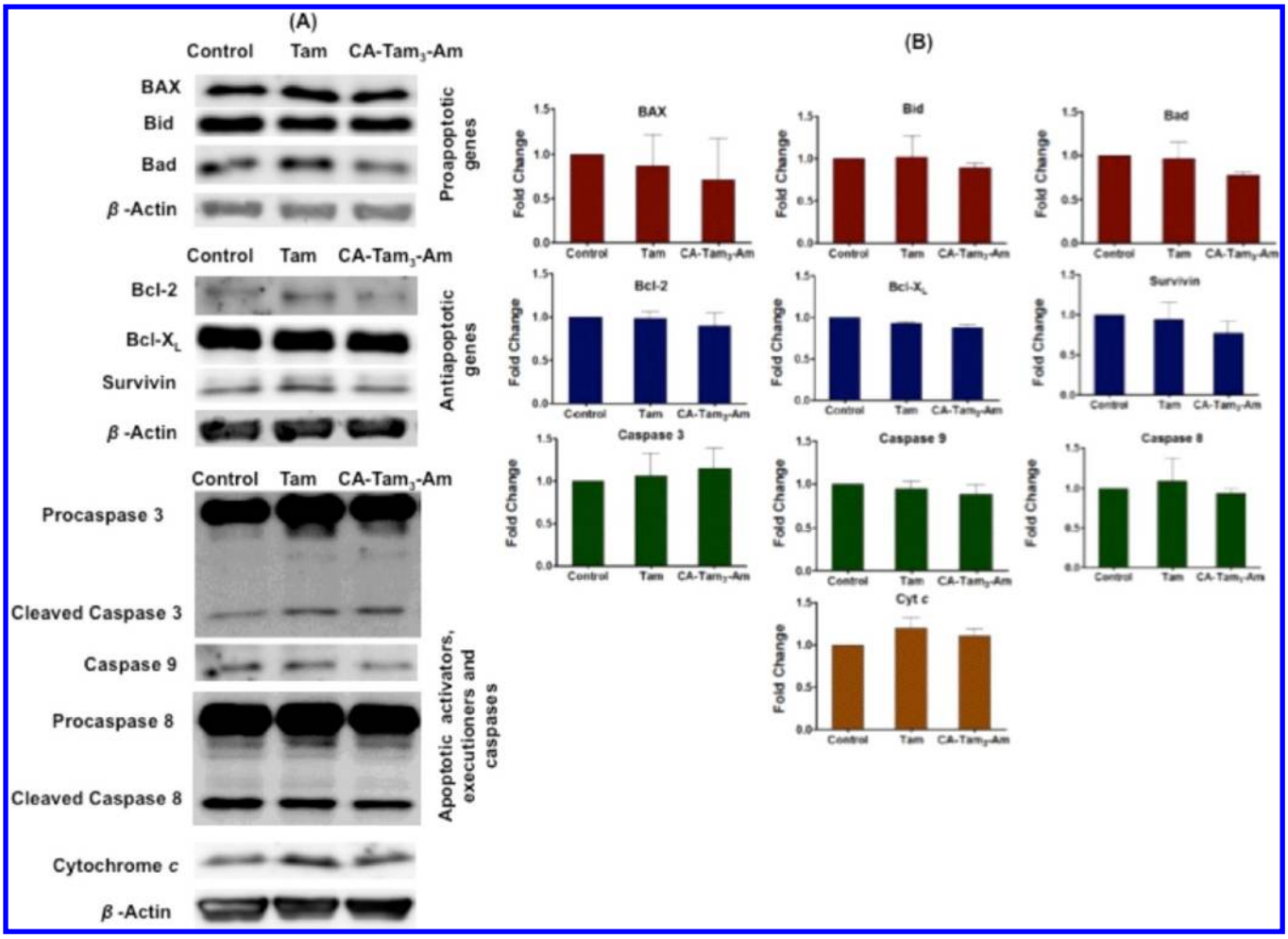

Figure 6. (A) Western blot studies of MDA-MB-231 cells treated with **Tam** and **CA-Tam$_3$-Am** at 10 μM tamoxifen equivalent concentration for 48 h. (B) Graphical representation of the densitometry of all proteins in Western blot performed in triplicate with mean ± SD. All of the values were normalized using β-actin as the internal control.

Quantitative Real Time PCR and Western Blotting Studies in ER +ve MCF-7 Cells. Real time PCR analysis showed that **CA-Tam$_3$-Am** causes down-regulation of anti-apoptotic Bcl-2 gene expression by 0.75-fold, whereas no effect was observed in Bcl-X$_L$ in ER +ve MCF-7 cells (Figure S6, Supporting Information). **CA-Tam$_3$-Am** causes a 1.2-, 1.8-, and 4.6-fold increase in the expression of Bax, Bid, and Bad genes, respectively, whereas tamoxifen treatment causes a 1.5-fold change for Bid and Bad and no change in mRNA levels for Bax. Tamoxifen and **CA-Tam$_3$-Am** treatment causes a 3.0-fold up-regulation of caspase 9 and 1.5-fold up-regulation of caspase 8 that is involved in the pathway of extrinsic apoptosis triggered by death receptors (Figure S6, Supporting Information). As caspase 8 promotes mitochondrial permeation of cytochrome *c* and in turn activates caspase 9 through cleavage of Bid, we found a 1.9-fold increase in levels of cytochrome *c* after **CA-Tam$_3$-Am** treatment, whereas tamoxifen treatment does not change mRNA levels of caspase 8 and cytochrome *c*. Tamoxifen and **CA-Tam$_3$-Am** down-regulate mRNA levels of Survivin by 10-fold, a member of the family inhibitors of apoptosis (IAPs), which is a critical component of apoptosis as it inhibits both Bax (intrinsic) and Fas induced (extrinsic) apoptosis.

Western studies showed down-regulation of antiapoptotic Bcl-2 and Bcl-X$_L$ protein levels and up-regulation of proapoptotic proteins Bax, Bid, Bad, and caspase 8 in MCF-7 cells upon treatment with **CA-Tam$_3$-Am** without change in the expression of caspase 9 (Figure 5), whereas after treatment with **Tam**, there is down-regulation of Bcl-2 (not Bcl-X$_L$), up-regulation of Bax and Bad (not Bid), and no change in levels of caspase 8 and caspase 9. We have observed elevated levels of cleaved caspases 8 on treatment with **CA-Tam$_3$-Am** (Figure 5). Among other proteins, Cytochrome *c* was up-regulated, and IAP family protein Survivin protein was down-regulated after treatment with **Tam** and **CA-Tam$_3$-Am**. We studied levels of caspase 3 by PCR and Western studies and found that it is not expressed in MCF-7 cells, which is in agreement with previous reports.[41−43] Absence of caspase 3 that is critical for apoptosis by the intrinsic apoptotic pathway and activation of caspase 8 critical for the extrinsic apoptotic pathway can allow MCF-7 cells to undergo apoptosis via death receptor mediated or the extrinsic pathway upon treatment with **CA-Tam$_3$-Am**. However, activation of proapoptotic genes Bax and Bad and down-regulation of antiapoptotic genes Bcl-2 and Bcl-X$_L$ can allow for the cells' induction of intrinsic apoptotic pathways in reponse to **CA-Tam$_3$-Am**. Therefore, these observations at mRNA and protein levels conclude that treatment of MCF-7 cells with **CA-Tam$_3$-Am** causes cell death via extrinsic as well as intrinsic pathways of apoptosis.

The intrinsic pathway of apoptosis, also known as mitochondrial pathway or stress pathway, is activated by a

dx.doi.org/10.1021/bc300664k | *Bioconjugate Chem.* 2013, 24, 1468−1484

diverse array of death stress, genomic stress, metabolic stress, the presence of unfolded proteins, and other stimuli. All these arrays lead to the permeabilization of the outer mitochondrial membrane and the release of apoptotic proteins from mitochondria into cytosol. Treatment of MCF-7 cells with **CA-Tam$_3$-Am** generates ROS and causes cytochrome *c* release from mitochondria to cytosol, which in turn induces a series of biochemical reactions that result in caspase activation and subsequent cell death.[44] Release of cytochrome *c* in response to excessive ROS generation can activate initiator caspase 9, which further activates executioner caspases 3, 6, and 7. Survivin is a family of inhibitor of apoptosis (IAP) protein and gets down-regulated and activates cells toward apoptosis by allowing the caspase cascade. Sequence of events including up-regulation of proapoptotic genes and caspases and down-regulation of antiapoptotic genes promote cells toward death. The extrinsic pathway, which is also known as death receptor induced pathway, also gets activated by initiator caspase 8, followed by cleavage and activation of Bid, dimerization of Bax, and further activation of caspases 3, 6, and 7 leading to cell death or apoptosis upon treatment with **CA-Tam$_3$-Am**.

Quantitative Real Time PCR and Western Blotting Studies in ER −ve MDA-MB-231 Cells. Real time PCR analysis of ER −ve MDA-MB-231 cells upon treatment with **CA-Tam$_3$-Am** showed up-regulation of pro-apoptotic genes Bax, Bid, and Bad to levels of 1.7-, 2.5-, and 3-fold, respectively (Figure S7, Supporting Information), whereas **Tam** treatment causes 1.25-, 0.8-, and 1.75-fold change for proapoptotic genes Bax, Bid, and Bad, respectively. There is no significant change in levels of Bcl-X$_L$ after tamoxifen and **CA-Tam$_3$-Am** treatment, whereas Bcl-2 levels were up-regulated indicating that treatment of estrogen receptor −ve MDA-MB-231 cells with tamoxifen and **CA-Tam$_3$-Am** does not down-regulate the expression of antiapoptotic Bcl-2 family proteins required for apoptosis. Treatment with tamoxifen and **CA-Tam$_3$-Am** induces up-regulation of caspase 9 and caspase 3 in MDA-MB-231 cells (Figure S7, Supporting Information), whereas only **CA-Tam$_3$-Am** up-regulates the levels of caspase 8. **CA-Tam$_3$-Am** also up-regulates levels of cytochrome *c* by 2.4-fold and down-regulates Survivin by 0.7-fold. Tamoxifen treatment increases mRNA levels by 1.25-fold for cytochrome *c* and causes no change for Survivin in MDA-MB-231 cells.

We then looked at the protein expression levels of the same genes (Figure 6) in MDA-MB-231 cells upon treatment with **Tam** and **CA-Tam$_3$-Am**. Contrary to our observations with mRNA expression levels, we have observed no up-regulation in protein expression levels of pro-apoptotic proteins Bax, Bid, and Bad in MDA-MB-231 cells, and only a marginal decrease in levels of antiapoptotic Bcl-2 and Bcl-X$_L$ levels was observed in response to **Tam** and **CA-Tam$_3$-Am** treatment. Among caspases, we have observed the up-regulation of caspase 3 and no up regulation in caspase 8 and caspase 9 levels after **Tam** and **CA-Tam$_3$-Am** treatment (Figure 6). We observed increased levels of cleavage products of caspase 3. Cytochrome *c* gets up-regulated, and Survivin gets down-regulated in MDA-MB-231 cells upon treatment with **Tam** and **CA-Tam$_3$-Am**.

Treatment of MDA-MB-231 cells with **CA-Tam$_3$-Am** causes an increase in levels of ROS and cytochrome *c*, followed by up-regulation of apoptotic genes as shown by mRNA levels making the cells undergo apoptosis. Generation of ROS is much higher in response to **CA-Tam$_3$-Am** treatment as compared to that with **Tam** in MDA-MB-231 cells, which is also higher as compared to that in MCF-7 cells. These results conclude that **CA-Tam$_3$-Am** treatment results in the generation of a higher amount of ROS inside mitochondria making the mitochondrial membrane more permeable to release cytochrome *c* that activates apoptosis. Release of cytochrome *c* activates and up-regulates many pro-apoptotic expression levels and caspases as evident from mRNA expression levels. The absence of changes in protein expression levels in MDA-MB-231 cells upon treatment with **CA-Tam$_3$-Am** also indicates a different mechanism of action for these cells to undergo apoptosis.

Anticancer activities in ER +ve MCF-7 and ER −ve MDA-MB-231 cells and their mechanistic investigation studies by PCR and Western studies showed that treatment of ER +ve MCF-7 cells with **CA-Tam$_3$-Am** induces cells to undergo apoptosis by extrinsic and intrinsic pathways through the regulation of apoptotic genes and caspases, whereas ER −ve MDA-MB-231 cells lines may undergo cell death using the intrinsic pathway as evident from mRNA expression levels.

***In Vivo* 4T1 Breast Cancer Model in Balb/c Mice.** We evaluated the antitumor potency of **CA-Tam$_3$-Am** *in vivo* in murine 4T1 breast cancer tumor models in Balb/c mice. We divided the animals bearing ∼150 mm^3 tumors in 3 groups consisting of 6 animals each. Animals were administered with DMSO vehicle control (100 μL), tamoxifen (15 mg/kg), and **CA-Tam$_3$-Am** (15 mg/kg tamoxifen equivalent dose) once a week. We observed that a single dose of **CA-Tam$_3$-Am** on day 7 was able to reduce the tumor burden by ∼50% within a week on day 13 (Figure 7), whereas a single dose of **Tam** did not show any change in the **Tam** treated group. Only the second dose of **Tam** was able to reduce the tumor burden by ∼30% on 16th day, whereas the **CA-Tam$_3$-Am** treated tumor showed ∼50% reduction in tumor volume. These studies showed that **CA-Tam$_3$-Am** is more potent than tamoxifen alone in murine breast cancer tumor models (Figure 7).

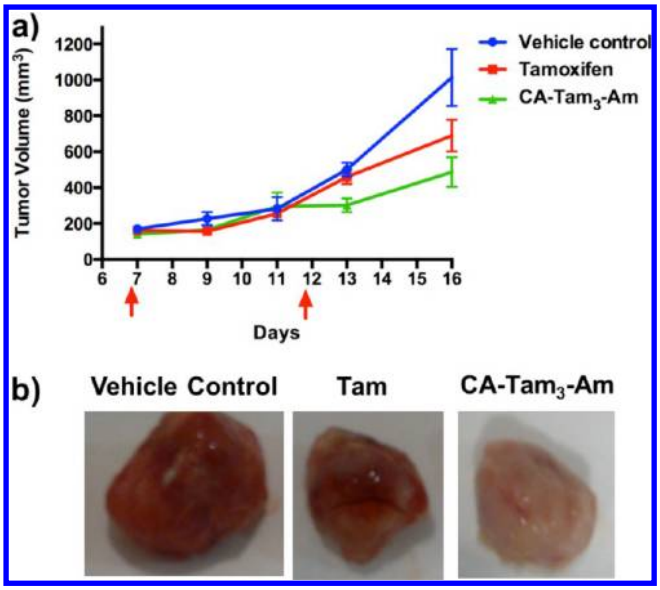

Figure 7. *In vivo* antitumor activity of **CA-Tam$_3$-Am** in the murine 4T1 breast cancer model in Balb/c mice. (a) Graph shows change in tumor volume in different treatment groups (n = 6 per group) in the 4T1 tumor model upon administration of the vehicle (100 μL), tamoxifen (15 mg/kg), **CA-Tam$_3$-Am** (15 mg/kg tamoxifen equivalent dose) weekly once (marked by red arrows). Graph was plotted with the mean ± SEM and statistical analysis done by ANOVA, $p < 0.005$. (b) Representative images of excised 4T1 tumors.

dx.doi.org/10.1021/bc300664k | *Bioconjugate Chem.* 2013, 24, 1468−1484

CONCLUSIONS

In this article, we present the synthesis of six bile acid−tamoxifen conjugates bearing acid and amine head groups and their anticancer activities and mechanistic studies in ER +ve and ER −ve breast cancer cells. The cholic acid−tamoxifen conjugate having three tamoxifen molecules and an amine headgroup, **CA-Tam$_3$-Am**, is the most active in both estrogen +ve and −ve cells. The mechanism for differential activities among bile acid−tamoxifen conjugates showed the reversible binding and lower impact on fluidization states of membranes by bile acid−tamoxifen compounds with acid head groups making them less active. Bile acid−tamoxifen compounds having amine head groups showed stable binding with membranes, and among these drug−liposome stable complexes, only **CA-Tam$_3$-Am** causes maximum disruptions in membranes causing higher membrane fluidity and penetration. Interestingly, SPR and DPH studies using bile acid−tamoxifen conjugates correlate with anticancer activities of these conjugates showing that acid conjugates of bile acid−tamoxifen are not active and that among amine conjugates, **CA-Tam$_3$-Am** is the most active. Annexin-V-FITC-PI studies confirmed that cells undergo apoptosis irrespective of ER status upon treatment with **CA-Tam$_3$-Am**, and cell cycle analysis showed sub G_0 arrest of cells. The ROS assay showed the generation of increased levels of ROS upon **CA-Tam$_3$-Am** treatment, which is independent of the ER status of cell lines. **CA-Tam$_3$-Am** treatment in MCF-7 cells down-regulates mRNA and protein levels of antiapoptotic Bcl-2, Bcl-X_L, and Survivin and up-regulates proapoptotic Bax, Bid, Bad, cytochrome *c*, and caspase 8 indicating intrinsic and extrinsic pathways of apoptosis. MDA-MB-231 cells upon treatment with **CA-Tam$_3$-Am** showed regulation of genes similar to MCF-7 cells at mRNA levels indicating an intrinsic pathway of apoptosis, but no change in levels of protein expression indicates a different mechanism of action in ER −ve cell lines. The *in vivo* studies in the murine 4T1 breast cancer model in Balb/c mice showed that **CA-Tam$_3$-Am** is a more potent molecule than tamoxifen causing ∼50% reduction in tumor volume with a single dose within a week. **CA-Tam$_3$-Am** can easily form liposomes and can be explored for *in vivo* applications using oral or intravenous delivery. We are currently developing strategies to engineer liposomes using **CA-Tam$_3$-Am** for effective delivery. In conclusion, we have shown that bile acid provides an excellent scaffold for drug delivery applications and that drug delivery strongly depends on the charge and hydrophobicity of the molecules that control its interactions with cell membranes.

ASSOCIATED CONTENT

Supporting Information

Percentage cell survival in the presence of **Tam** and bile acid−tamoxifen conjugates having acid head groups, amine head groups; percentage cell survival in the presence of **Tam**, **CA-Tam$_3$-Am**, and a physical mixture of cholic acid amine and tamoxifen in MCF-7 (ER +ve) and MDA-MB-231 (ER −ve) cell lines; concentration dependent drug binding responses of **Tam** and bile acid−tamoxifen conjugates at different concentrations; generation of reactive oxygen species using the DCFDA method; and quantitative real time PCR of MCF-7 and MDA-MB 231 cells treated with **Tam** and **CATam$_3$- Am**. This material is available free of charge via the Internet at http://pubs.acs.org.

AUTHOR INFORMATION

Corresponding Author

*Phone: +91-124-2848831. Fax: +91-124-4038117. E-mail: bajaj@rcb.res.in.

Author Contributions

[§]V.S. and S.B. contributed equally to this work.

Notes

The authors declare no competing financial interest.

ACKNOWLEDGMENTS

We thank RCB for intramural funding and Department of Biotechnology for supporting this project. A.B. thanks Department of Science and Technology for Ramanujan Fellowship. V.S. and S.K. thank RCB for the research fellowship. We thank Dr. Monica Sundd, NII for helping us in initial NMR studies, AIRF JNU for the NMR facility, Vishakha Chaudhary for helping in mass spectra analysis, and Atin Jaiswal for help in SPR measurements.

ABBREVIATIONS

CA, cholic acid; DCA, deoxycholic acid; DPPC, dipalmitoylphosphatidylcholine; DPH, diphenylhexatriene; ER, estrogen receptor; LCA, lithocholic acid; SPR, surface plasmon resonance

REFERENCES

(1) Chabner, B. A., and Roberts, T. G., Jr. (2005) Chemotherapy and the war on cancer. *Nat. Rev. Cancer 5*, 65−72.

(2) Rosen, H., and Abribat, T. (2005) The rise and rise of drug delivery. *Nat. Rev. Drug Discovery 4*, 381−385.

(3) Allen, T. M., and Cullis, P. R. (2004) Drug delivery systems: entering the mainstream. *Science 303*, 1818−1822.

(4) Lerner, B. H. (2002) Breast cancer activism: past lessons, future directions. *Nat. Rev. Cancer 2*, 225−230.

(5) Jordan, V. C. (2003) Tamoxifen: a most unlikely pioneering medicine. *Nat. Rev. Drug Discovery 2*, 205−213.

(6) Jain, A. K., Swarnakar, N. K., Godugu, C., Singh, R. P., and Jain, S. (2011) The effect of the oral administration of polymeric nanoparticles on the efficacy and toxicity of tamoxifen. *Biomaterials 32*, 503−515.

(7) Sengupta, P., Basu, S., Soni, S., Pandey, A., Roy, B., Oh, M. S., Chin, K. T., Paraskar, A. S., Sarangi, S., Connor, Y., Sabbisetti, V. S., Kopparam, J., Kulkarni, A., Mutoc, K., Amarasiriwardena, C., Jayawardene, I., Lupoli, N., Dinulescu, D. M., Bonventre, J. V., Mashelkar, R. A., and Sengupta, S. (2012) Cholesterol-tethered platinum II-based supramolecular nanoparticle increases antitumor efficacy and reduces nephrotoxicity. *Proc. Natl. Acad. Sci. U.S.A. 109*, 11294−11299.

(8) Chhikara, B. S., Mandal, D., and Parang, K. (2012) Synthesis, anticancer activities, and cellular uptake studies of lipophilic derivatives of doxorubicin succinate. *J. Med. Chem. 55*, 1500−1510.

(9) Agarwal, H. K., Chhikara, B. S., Bhavaraju, S., Mandal, D., Doncel, G. F., and Parang, K. (2013) emtricitabine prodrugs with improved anti-HIV activity and cellular uptake. *Mol. Pharmacol. 10*, 467−476.

(10) Pal, K., Pore, S. K., Sinha, S., Janardhanan, R., Mukhopadhyay, D., and Banerjee, R. (2011) Structure−activity study to develop cationic lipid-conjugated haloperidol derivatives as a new class of anticancer therapeutics. *J. Med. Chem. 54*, 2378−2390.

(11) Sinha, S., Roy, S., Reddy, B. S., Pal, K., Sudhakar, G., Iyer, S., Dutta, S., Wang, E., Vohra, P. K., Roy, K. R., Reddanna, P., Mukhopadhyay, D., and Banerjee, R. (2011) A lipid-modified estrogen derivative that treats breast cancer independent of estrogen receptor expression through simultaneous induction of autophagy and apoptosis. *Mol. Cancer Res. 9*, 364−374.

(12) Mukhopadhyay, S., and Maitra, U. (2004) Chemistry and biology of bile acids: a review. *Curr. Sci. 87*, 1666−1683.
(13) Tolle-Sander, S., Lentz, K. A., Maeda, D. Y., Coop, A., and Polli, J. E. (2003) Increased acyclovir oral bioavailability *via* a bile acid conjugate. *Mol. Pharm. 1*, 40−48.
(14) Briz, O., Serrano, M. A., Rebollo, N., Hagenbuch, B., Meier, P. J., Koepsell, H., and Marin, J. J. G. (2002) Carriers involved in targeting the cytostatic bile acid-cisplatin derivatives cis-diammine-chloro-cholylglycinate-platinum(II) and cis-diammine-bisursodeoxycholate-platinum(II) toward liver cells. *Mol. Pharmacol. 61*, 853−860.
(15) Xiao, K., Lio, J., Fowler, W., Li, Y., Lee, J., and Wang, L. (2009) A self-assembling nanoparticle for paclitaxel delivery in ovarian cancer. *Biomaterials 30*, 6006−6016.
(16) Bajaj, A., Kondaiah, P., and Bhattacharya, S. (2008) Synthesis and gene transfection efficacies of PEI-cholesterol-based lipopolymers. *Bioconjugate Chem. 19*, 1640−1651.
(17) Bhattacharya, S., and Bajaj, A. (2007) Thermotropic and hydration Studies of membranes formed from gemini pseudoglyceryl lipids possessing polymethylene spacers. *Langmuir 23*, 8988−8994.
(18) Rich, R. L., and Myszka, D. G. (2000) Advances in surface plasmon resonance biosensor analysis. *Curr. Opin. Biotechnol. 11*, 54−61.
(19) Ghosh, Y. K., Indi, S. S., and Bhattacharya, S. (2001) Thermal lipid order-disorder transitions in mixtures of cationic cholesteryl lipid analogues and dipalmitoyl phosphatidylcholine membranes. *J. Phys. Chem. B 105*, 10257−10265.
(20) Dreaden, E. C., Mwakwari, S. C., Sodji, Q. H., Oyelere, A. K., and El-Sayed, M. A. (2009) Tamoxifen poly(ethylene glycol)-thiol gold nanoparticle conjugates: enhanced potency and selective delivery for breast cancer treatment. *Bioconjugate Chem. 20*, 2247−2253.
(21) Zhang, G., Kimijima, I., Onda, M., Kanno, M., Sato, H., Watanabe, T., Tsuchiya, A., Abe, R., and Takenoshita, S. (1999) Tamoxifen-induced apoptosis in breast cancer cells relates to down-regulation of bcl-2, but not bax and bcl-XL without alteration of p53 protein levels. *Clin. Cancer Res. 5*, 2971−2977.
(22) O'Brian, C. A., Liskamp, R. M., Solomon, D. H., and Weinstein, I. B. (1986) Triphenylethylenes: a new class of protein kinase C inhibitors. *J. Natl. Cancer Inst. 76*, 1243−1246.
(23) Vereb, G., Szollosi, J., Matko, J., Nagy, P., Farkas, T., Vigh, L., Matyus, L., Waldmann, T. A., and Damjanovich, S. (2003) Dynamic, yet structured: the cell membrane three decades after the Singer-Nicolson model. *Proc. Natl. Acad. Sci. U.S.A. 100*, 8053−8058.
(24) Abdiche, Y. N., and Myszka, D. G. (2004) Probing the mechanism of drug/lipid membrane interactions using Biacore. *Anal. Biochem. 328*, 233−243.
(25) Tsai, H., Lin, L., Lai, Z., Wu, J., Chen, C., Hwang, J., Chen, C., and Lin, C. (2010) Immobilizing topoisomerase I on a surface plasmon resonance biosensor chip to screen for inhibitors. *J. Biomed. Sci. 17*, 49−57.
(26) Rich, R. L., Hoth, L. R., Geoghegan, K. F., Brown, T. A., LeMotte, P. K., Simons, S. P., Hensley, P., and Myszka, D. G. (2002) Kinetic analysis of estrogen receptor/ligand interactions. *Proc. Natl. Acad. Sci. U.S.A. 99*, 8562−8567.
(27) Danelian, E., Karlen, A., Karlsson, R., Winiwarter, S., Hansson, A., Lofas, S., Lennernas, H., and Hamalainen, M. D. (2000) SPR Biosensor studies of the direct interaction between 27 drugs and a liposome surface: correlation with fraction absorbed in humans. *J. Med. Chem. 43*, 2083−2086.
(28) Crielaard, B. J., Yousefi, A., Schillemans, J. P., Vermeheren, C., Buyens, K., Braeckmans, K., Lammers, T., and Storm, G. (2011) An in vitro assay based on surface plasmon resonance to predict the in vivo circulation kinetics of liposomes. *J. Controlled Release 156*, 307−314.
(29) Austin, R. P., Barton, P., Davis, A. M., Fessey, R. E., and Wenlock, M. C. (2005) The thermodynamics of the partitioning of ionizing molecules between aqueous buffers and phospholipid membranes. *Pharm. Res. 22*, 1649−1657.
(30) Sykes, M. J., Sorich, M. J., and Miners, J. O. (2006) Molecular modeling approaches for the prediction of the nonspecific binding of drugs to hepatic microsomes. *J. Chem. Inf. Model. 46*, 2661−2673.
(31) Nussio, M. R., Sykes, M. J., Miners, J. O., and Shapter, J. G. (2007) Characterization of the binding of cationic amphiphilic drugs to phospholipid bilayers using surface plasmon resonance. *ChemMedChem 2*, 366−373.
(32) Peetla, C., Stine, A., and Labhasetwar, V. (2009) Biophysical interactions with model lipid membranes: applications in drug discovery and drug delivery. *Mol. Pharmaceutics 6*, 1264−1276.
(33) Lopes, S., Simeonova, M., Gamerio, P., Rangel, M., and Ivanova, G. (2012) Interaction of 5-fluorouracil loaded nanoparticles with 1,2-dimyristoyl-sn-glycero-3-phosphocholine liposomes used as a cellular membrane model. *J. Phys. Chem. B 116*, 667−675.
(34) Singh, M., Singh, A., Kundu, S., Bansal, S., and Bajaj, A. (2013) Deciphering the role of charge, hydration, and hydrophobicity for cytotoxic activities and membrane interactions of bile acid based facial amphiphiles. *Biochim. Biophys. Acta 1828*, 1926−1937.
(35) Sreekanth, V., and Bajaj, A. (2013) Fluorescence (fluidity/hydration) and calorimetric studies of interactions of bile acid-drug conjugates with model membranes. *J. Phys. Chem. B 117*, 2123−2133.
(36) Sutherland, R. L., Hall, R. E., and Taylor, I. W. (1983) Cell proliferation kinetics of MCF-7 human mammary carcinoma cells in culture and effects of tamoxifen on exponentially growing and plateau-phase cells. *Cancer Res. 43*, 3998−4006.
(37) Waris, G., and Ahsan, H. (2006) Reactive oxygen species: role in the development of cancer and various chronic conditions. *J. Cancinogenesis 5*, 14−21.
(38) Kallio, A., Zheng, A., Dahllund, J., Heiskanen, K. M., and Harkonen, P. (2005) Role of mitochondria in tamoxifen-induced rapid death of MCF-7 breast cancer cells. *Apoptosis 10*, 1395−1410.
(39) Adams, J. M. (2003) Ways of dying: multiple pathways to apoptosis. *Genes Dev. 17*, 2481−2495.
(40) Razandi, M., Pedram, A., Jordan, V. C., Fuqua, S., and Levin, E. R. (2012) Tamoxifen regulates cell fate through mitochondrial estrogen receptor beta in breast cancer. *Oncogene 32*, 3274−3285.
(41) Reiner, U. J. (2009) MCF-7 Breast carcinoma cells do not express caspase 3. *Breast Cancer Res. Treat. 117*, 219−221.
(42) Liang, Y., Yan, C., and Schor, F. N. (2001) Apoptosis in the absence of caspase 3. *Oncogene 20*, 6570−6578.
(43) Kagawa, S., Gu, J., Honda, T., McDonnell, T. J., Swisher, S. G., Roth, J. A., and Fang, B. (2001) Deficiency of Caspase-3 in MCF7 cells blocks Bax-mediated nuclear fragmentation but not cell death. *Clin. Cancer Res. 7*, 1474−1480.
(44) Jiang, X., and Wang, X. (2004) Cytochrome c mediated apoptosis. *Annu. Rev. Biochem. 73*, 87−106.